Oceanologia (2018) 60, 32—51

Available online at www.sciencedirect.com

ScienceDirect

journal homepage: www.journals.elsevier.com/oceanologia/

ORIGINAL RESEARCH ARTICLE

Modeling the ecosystem response to summer coastal upwelling in the northern South China Sea

Rui Jiang [a,b], **You-Shao Wang** [a,c,*]

[a] *State Key Laboratory of Tropical Oceanography, South China Sea Institute of Oceanology, Chinese Academy of Sciences, Guangzhou, China*
[b] *University of Chinese Academy of Sciences, Beijing, China*
[c] *Daya Bay Marine Biology Research Station, Chinese Academy of Sciences, Shenzhen, China*

Received 19 October 2016; accepted 19 May 2017
Available online 15 June 2017

KEYWORDS
The northern South China Sea;
NPZD ecosystem model;
Summer coastal upwelling;
Coastal ecosystem

Summary A coupled three-dimensional physical model and a nitrogen-based nutrient, phytoplankton, zooplankton, and detritus (NPZD) ecosystem model were applied to simulate the summer coastal upwelling system over the continental shelf of northern South China Sea (NSCS) and its impact on hydrographic conditions and ecosystem. The simulated results were comprehensively validated against field and satellite measurements. The model results show that the near shore ecosystem of NSCS has significant responses to the summer coastal upwelling system. The Shantou Coast to the Nanri Islands of Fujian province (YD) and the east of the Leizhou Peninsula (QD) are two main regions affected by NSCS summer coast upwelling. During summer, these two coastal areas are characterized by nearshore cold and high salinity upwelling current. Further, the summer coastal upwelling serves as a perfect nutrient pump, which lifts up and advects nutrient-rich current from deep to surface, from inner shelf to about 30 km outer shelf. This nutrient source reaches its maximum in the middle of July and then begins to decrease. However, the maximum phytoplankton and chlorophyll *a* do not coincide with the maximum nutrients and delay for about 10 days. Because of the intensive seasonal thermocline and the complicated current transporting through Qiongzhou strait, the ecological responding of QD is less pronounced than YD. This study has a better understanding of the physically modulated ecological responses to the NSCS summer coastal upwelling system.

* Corresponding author at: State Key Laboratory of Tropical Oceanography, South China Sea Institute of Oceanology, Chinese Academy of Sciences, Guangzhou 510301, China. Tel.: +86 20 8902 3102; fax: +86 20 8902 3102.
E-mail address: yswang@scsio.ac.cn (Y.-S. Wang).
Peer review under the responsibility of Institute of Oceanology of the Polish Academy of Sciences.

Production and hosting by Elsevier

http://dx.doi.org/10.1016/j.oceano.2017.05.004

1. Introduction

Coastal upwelling is one of the most prominent marine physical processes involving biogeochemical cycles, primary productivity, and fisheries (Prego et al., 2007). Coastal upwelling system is commonly produced by the interaction between favorable winds and the topography (Woodson et al., 2007) and is characterized by bringing cold and nutrient-rich deep water toward the surface while influencing the transport of suspended matters (Freon et al., 2009). Because of its important role in the marine ecosystem, coastal upwelling has been studied worldwide (González-Gil et al., 2015; Ruzicka et al., 2016).

The South China Sea (SCS) is located in the southeast of Asia with an average depth of about 1350 m. It is the largest marginal sea in the world, which stretches 3.5×10^6 km^2 from 23°57′N in the north to the 3°00′N in the south and from 99°10′E in the west to the 122°10′E in the east (Chen et al., 2006). The SCS also supports the most frequent human activity (Li et al., 2014). Our study area — northern South China Sea (NSCS) (Fig. 1) is affected by both natural environment and human activities year-round. In the northern shelf of the NSCS, there are many rivers which input fresh water into it (such as the Pearl River), while the south of the NSCS joins to the SCS. The occurrence of summer coastal upwelling is a regular phenomenon during June to September in the NSCS, and there are two main coastal upwelling regions: Shantou Coast to the Nanri Islands of Fujian province (YD), and the east of the Leizhou Peninsula (QD) (Jing et al., 2008). All of these days, temperature, salinity, dissolved oxygen (DO) and chlorophyll *a* have been regarded as four main indicators for NSCS summer coastal upwelling (Wang, 2013). In order to explore the corresponding environmental changes, a lot of research techniques have been used, such as remote sensing, multivariate statistical analysis, and indicator (silicate) method (Ehlert et al., 2013). However, the influence of the coastal upwelling system on the NSCS ecosystem is still not well understood because of the complex topography, currents and the dynamic climatology (Morton and Blackmore, 2000).

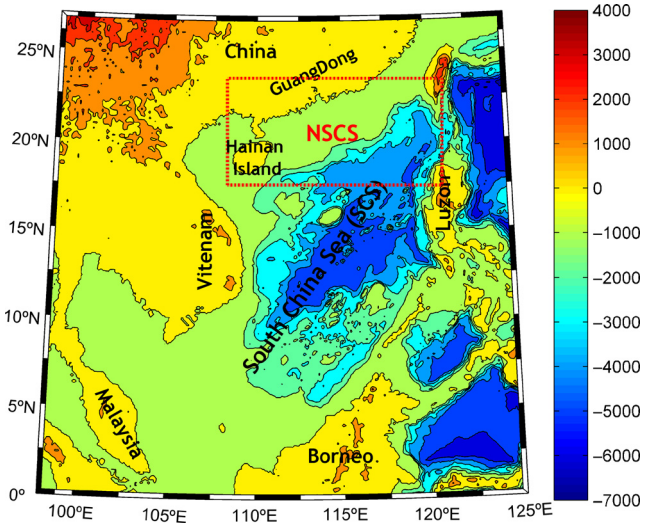

Figure 1 The northern South China Sea (NSCS) and its physiography; different colors represent the bathymetry of the South China Sea [altitude: m]. (For interpretation of the references to color in this figure legend, the reader is referred to the web version of this article.)

With increasing pressure for a profound understanding of marine ecosystems, numerical modeling becomes a powerful tool for research. Ecological models are ecosystem-based management tools that can be used to forecast ecological impacts. Through their ability to integrate into in situ measurements with the theoretical assumptions of ecosystem response, ecological models can be an effective tool for developing strategies for simulating the environmental changes (Cropper and DiResta, 1999). Coupled physical-biological model can be an efficient approach to study the time dependent three-dimensional responses of the marine ecosystem to the coastal upwelling system, and it can also compensate the time-space restrictions of the earlier studies.

In the paper, the Regional Ocean Model System (ROMS) coupled with a nitrogen-based nutrient, phytoplankton, zooplankton, and detritus (NPZD) ecosystem model was given in the NSCS, and was also constructed and analyzed by discretization, driven condition, and validation methods.

2. Material and methods

2.1. Model description

The first generation of marine ecosystem models was put forward by Riley (Riley and Stommel, 1949), and constructed as a one-dimensional NP ecological model, which not only put phytoplankton, zooplankton as state variables, but also took photosynthesis, predator-prey relationship, and mineralization into account. It is also the foundation of the NPZD ecological model used in this paper. Compared with the NP model, this NPZD model describes ecosystem structure and functions in more detail, in addition, it is three-dimensional.

The NPZD ecological model is one of the most popular models by virtue of its fewer requirements for parameters and observation data (Heinle and Slawig, 2013). It has successfully simulated many ecological and physical processes in different seas, for instance, the NPZD model was used to illustrate the relationship between changes in the intensity of the spring bloom and changes in the physical forcing in the northeast Atlantic Ocean (Waniek, 2003) and it was also used for simulating the long-term change of planktonic ecosystems in the upstream Kuroshio Current (Li et al., 2015).

The schematic of the NPZD ecological model is presented here (Fig. 2). It describes the evolution of nutrients (*N*), phytoplankton (*P*), zooplankton (*Z*) and detritus (*D*) (Powell et al., 2006). Furthermore, it is a nitrogen-based model and each square in it represents an ecological variable. These ecological variables belong to four submodules corresponding to *N* submodule, *P* submodule, *Z* submodule, and *D* submodule, respectively, and the arrows between the squares indicate directions of energy flows. Nutrients enter the sea through rivers and atmospheric precipitation transport. On one hand, phytoplankton utilizes photosynthesis for compounding organics for its autotrophic growth. But on the other hand, its growth is also limited by light, nutrients, and temperature, etc. Zooplankton is an important linkage

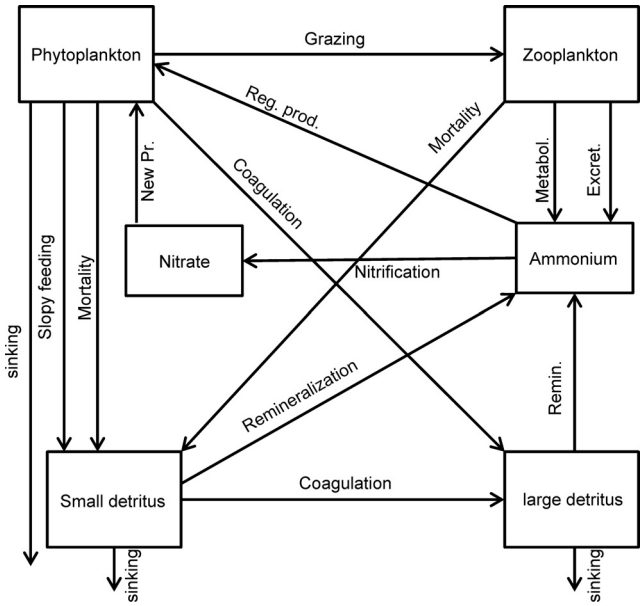

Figure 2 Schematic representation of the NPZD ecological model.

for energy transfer within the trophic structure of marine ecosystems (Turner and Tester, 1997). Zooplankton grazes the living phytoplankton and then assimilates it as its own organics. The unassimilated part, dead phytoplankton, dead zooplankton, and its excrement convert into detritus. As the last part, the new round of marine ecological cycle begins with detritus breaking down into nutrients.

2.2. NPZD model set-up

In this paper, the ecological model over the NSCS is the Fasham-type model (Fasham et al., 1990), which is embedded in the Regional Ocean Modeling System (ROMS). It is a nitrogen-based ecosystem model, which includes six prognostic variables: nitrate (NO_3), ammonium (NH_4), phytoplankton (*Phyto*), zooplankton (*Zoo*), large detritus (*LDetN*), and small detritus (*SDetN*). The NPZD model equations used in the paper can be written as follows:

$$\frac{\partial[NO_3]}{\partial t} = -t_{pp_{\max}}\cdot Q_{NP}\cdot[Phyto] + Q_{nitr}\cdot[NH_4], \tag{1}$$

$$\frac{\partial[NH_4]}{\partial t} = -t_{pp_{\max}}\cdot Q_{RP}\cdot[Phyto] - Q_{nitr}\cdot[NH_4] + (t_{Zbmet} + Q_{excr})\cdot[Zoo] + t_{SDremin}\cdot[SDetN] + t_{LDremin}\cdot[LDetN], \tag{2}$$

$$\frac{\partial[Phyto]}{\partial t} = t_{pp_{\max}}\cdot(Q_{NP} + Q_{RP})\cdot[Phyto] - t_{P_{mort}}\cdot[Phyto] - Q_{coag}\cdot[Phyto] - Q_{graze}\cdot[Zoo] + L_{vs}, \tag{3}$$

$$\frac{\partial[Zoo]}{\partial t} = Q_{graze}\cdot AE_N\cdot[Zoo] - t_{Zbmet}\cdot[Zoo] - t_{Zmort}\cdot[Zoo] - Q_{excr}\cdot[Zoo], \tag{4}$$

$$\frac{\partial[LDetN]}{\partial t} = t_{coag}\cdot([SDetN] + [Phyto])\cdot([SDetN] + [Phyto]) - t_{LDremin}\cdot[LDetN] + L_{vs}, \tag{5}$$

$$\frac{\partial[SDetN]}{\partial t} = Q_{graze}\cdot(1 - AE_N)\cdot[Zoo] + t_{pmort}\cdot[Phyto] + t_{Zmort}\cdot[Zoo] - t_{coag}\cdot([SDetN] + [Phyto])\cdot[SDetN] - t_{SDremin}\cdot[SDetN] + L_{vs}, \tag{6}$$

$$\frac{\partial(\theta)}{\partial t} = t_{PP_{\max}}\cdot(Q_{NP} + Q_{RP})\cdot\left(\frac{\theta_m\cdot V_p\cdot(Q_{NP} + Q_{RP})}{\sqrt{V_p^2 + \alpha^2\cdot\theta^2\cdot PAR^2}} - \theta\right) + L_{vs}, \tag{7}$$

$$Q_{NP} = \frac{([NO_3]/K_{NO_3})\cdot I_{NH_4}}{1 + [NO_3]/K_{NO_3}}, \tag{8}$$

$$Q_{RP} = \frac{[NH_4]/K_{NH_4}}{1 + [NH_4]/K_{NH_4}}, \tag{9}$$

$$Q_{nitr} = t_{nitri}\cdot\left(1 - \max\left[0, \frac{PAR - I_{thNH_4}}{D_{p5NH_4} + PAR - 2\cdot I_{thNH_4}}\right]\right), \tag{10}$$

$$Q_{graze} = t_{Z_{graze}}\cdot\frac{[Phyto]}{K_P + [Phyto]}, \tag{11}$$

$$Q_{excr} = Q_{graze}\cdot r_{C:N,phyto}\cdot AE_N\cdot\left(\frac{1}{r_{C:N,phyto}} - \frac{GGE_C}{AE_N\cdot r_{C:N,zoo}}\right), \tag{12}$$

$$I_{NH_4} = \frac{1}{1 + [NH_4]/K_{NH_4}}, \tag{13}$$

$$t_{PP_{\max}} = \frac{V_P\cdot\alpha\cdot PAR\cdot\theta}{\sqrt{V_p^2 + \alpha^2\cdot\theta^2\cdot PAR^2}}, \tag{14}$$

$$V_p = 0.59\cdot 1.066^T. \tag{15}$$

The parameters in these equations can be checked in Table 1. L_{vs} represents the vertical sinking terms, which affects phytoplankton, small and large detritus (ω_{Phyt}, ω_{SD}, ω_{LD}). All source terms ($Q\ldots$) are written such that they are non-dimensional.

Within the biology routine, the photosynthetically active radiation (*PAR*) for each cell is successively calculated. The loop starts at the top cell. For each cell, the *PAR* in the center of the cell is calculated with:

$$PAR_k = PAR_{k+1}\cdot e^{-0.5\cdot\left(k_{water} + k_{Chla}\cdot\lfloor Chla\rfloor_k\cdot\Delta z_k\right)},$$

k is the cell index (from 1 at the bottom to N at the top). PAR_{N+1} is the surface *PAR*, k_{water} and k_{Chla} are attenuation coefficient for water and chlorophyll, [*Chla*] is the chlorophyll

Table 1 List of parameters used in the biogeochemical model.

Variable	Description	Value	Unit
k_{water}	Light attenuation due to sea water	0.04	[m^{-1}]
K_{Chla}	Light attenuation by chlorophyll	0.024	[(m^2 mg *Chla*)$^{-1}$]
A	Initial slope of the *P–I* curve	1	[mg C (mg *Chla* W m^{-2} d)$^{-1}$]
$r_{C:N,phyto}$	C:N ratio for phytoplankton	6.625	[mol C (mol N)$^{-1}$]
$r_{C:N,zoo}$	C:N ratio for zooplankton	5	[mol C (mol N)$^{-1}$]
θ_m	Maximum cellular chlorophyll:C ratio	0.053478	[mg *Chla* (mg C)$^{-1}$]
K_{NO_3}	Half-saturation for phyto. NO_3 uptake	1.0/0.75	[mmol N m^{-3}]
K_{NH_4}	Half-saturation for phyto. NH_4 uptake	1.0/0.5	[mmol N m^{-3}]
t_{Pmort}	Phyt mortality to SDetN rate	0.072	[d^{-1}]
t_{Zgraze}	Zoo-specific maximum grazing rate	0.6	[d^{-1}]
AE_N	Zoo assimilation efficiency for N	0.75	[–]
K_P	Zoo half-saturation const. for ingestion	3	[mmol N m^{-3}]
t_{Zbmet}	Zoo specific excretion rate	0.1	[d^{-1}]
t_{Zmort}	Zoo quadratic mortality to Detritus	0.025	[d^{-1} (mmol N m^{-3})$^{-1}$]
$t_{SDremin}$	Small detrital breakdown to NH_4 rate	0.03	[d^{-1}]
$t_{LDremin}$	Specific rate of LDetN recycling to NH_4	0.01	[d^{-1}]
ω_{SD}	Sinking velocity for SDetN	1.0	[m d^{-1}]
ω_{LD}	Sinking velocity for LDetN	10	[m d^{-1}]
ω_{Phyto}	Sinking velocity for Phyt	0.5	[m d^{-1}]
t_{nitri}	Nitrification of NH_4 to NO_3	0.05	[d^{-1}]
D_{p5NH_4}	0.5 dose for nitrification inhibition	0.036	[W m^{-2}]
I_{thNH_4}	Threshold PAR for nutrition inhib	0.0095	[W m^{-2}]
t_{coag}	Specific (per unit Phyt + SDetN) aggregation rate	0.01	[(mmol N m^{-3})$^{-1}$ d^{-1}]
GGE_C	Zoo gross growth efficiency for C	0.65	[–]

concentration in this cell, and Δ_{zk} is the height of the cell. After the calculation of the newly generated production, PAR_k is multiplied again with the same attenuation factor.

2.3. Coupling NPZD ecological model with physical model

The adopted physical model — ROMS is a new generation ocean circulation model (Shchepetkin and McWilliams, 2005) that has been specially designed for accurate simulations of regional oceanic systems.

ROMS is discretized in coastline and terrain-following curvilinear coordinates using high-order numerical methods. It is a split-explicit, free-surface ocean model, where short time steps are used to advance the surface elevation and barotropic momentum, with a much larger time step used for temperature, salinity, and baroclinic momentum. The model has a 2-way time-averaging procedure for the barotropic mode, which satisfies the 3D continuity equation. The specially designed 3rd order predictor-corrector time step algorithm allows a substantial increase in the permissible time-step size (Shchepetkin and McWilliams, 1998). To address the challenge of bridging the gap between near-shore and off-shore dynamics, a nesting capability has been added to ROMS and tested for the California Upwelling System (Davenport et al., 2012; Penven et al., 2006).

ROMS can be used to process the initial conditions and lateral boundary conditions for biogeochemical tracer. It can assist in adding initial and lateral conditions for biogeochemical variables of the NPZD model.

2.4. Data

In this paper we use World Ocean Altas 2009 (WOA2009) global dataset (monthly climatology at 1° resolution), CSIRO Atlas of Regional Seas (CARS2009) database (annual, seasonal and monthly climatology for temperature, salinity, nitrate, phosphate, and oxygen), and COADS05 (directory of the surface fluxes global monthly climatology at 0.5° resolution). Besides, surface chlorophyll *a* climatology is based on SeaWiFS observation.

WOA2009 or CARS2009 provides a monthly, seasonal and annual climatology for nitrate concentration, phosphate, silicate, and oxygen. WOA or SeaWiFS can then be used to obtain climatology of surface chlorophyll concentration. Phytoplankton is estimated by a constant chlorophyll/phytoplankton ratio derived from previous simulations, and zooplankton is estimated in a similar way ($Chla/P = 1.59$; $Z/P = 0.3$) (Gan et al., 2009a,b).

3. Model discretization and the driven condition

3.1. Model discretization

In this study, the model was run for 3 years and initialized after a 10-year long spin-up (Powell et al., 2006) to ensure a steady state. The model was configured over the NSCS region (107°00′–121°E; 17°00′–23°30′N) and open boundaries were given in east, west and south boundaries of the domain

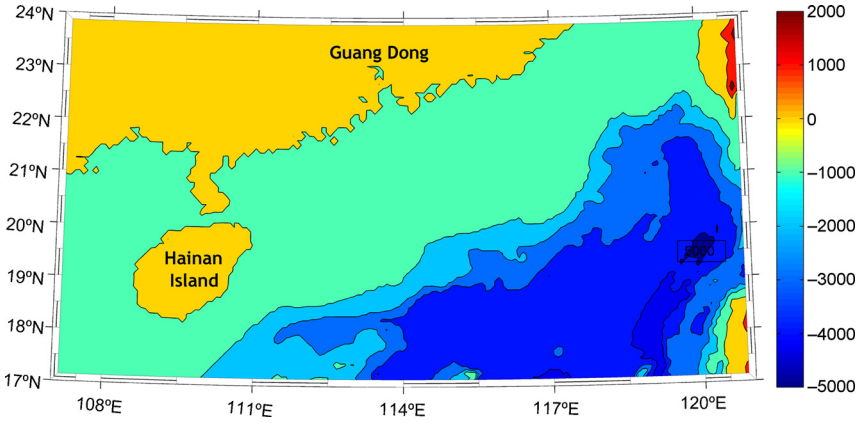

Figure 3 The northern South China Sea (NSCS) model domain and bathymetry; different colors represent the bathymetry of the NSCS [altitude: m]. (For interpretation of the references to color in this figure legend, the reader is referred to the web version of this article.)

(Fig. 3); meanwhile, the radiation open boundary conditions for barotropic velocities and mass conservation enforcement were used. The horizontal resolution of the model is 20.8 km, which is enough to resolve the first and second baroclinic Rossby deformation radius in the basin (Chelton et al., 1998). In vertical, the simulated domain is discretized into 32 vertical levels. Furthermore, the spatial resolution of the model is 1/5 and the time step is 3600 s.

3.2. Model driven condition

The model driven condition contains different surface fluxes, such as wind stress, surface net heat flux, surface freshwater flux, sea surface temperature, solar shortwave radiation, and sea surface salinity, etc.

The wind stress vectors and wind stress norm were obtained from the global atlas of surface marine data at 1/2° resolution at 4 different periods of the year (Fig. 4b). Sea surface temperature (SST) is used for the restoring term in the heat flux calculation (Fig. 4a). To improve the model solution, it is possible to use SST climatology at a finer resolution (9.28 km) (Casey and Cornillon, 1999). For the surface forcing, instead of directly prescribing the fluxes, it is possible to use a bulk formula to generate the surface fluxes from atmospheric variables during the model run.

4. Model validation procedure and criteria

As the basis of this coupled model, the accuracy of the hydrodynamic model is of great importance to the NPZD model. To assess it, the hydrodynamic model results were compared with Simple Ocean Data Assimilation analytic system (https://climatedataguide.ucar.edu/climate-data/soda-simple-ocean-data-assimilation) (SODA-an ocean reanalysis database). The simulated seasonal changes of sea surface temperature and flow field show a reasonable agreement with SODA (Figs. 5 and 6). Furthermore, to give this hydrodynamic model a quantitative validation, the Root Mean Square Error (RMSE) and correlation coefficient (Corrcoef) of the sea surface flow velocities (X direction of the flow in YD (u(YD)) and QD (u(QD)), Y direction of the flow in YD (v(YD)) and QD (v(QD))) between the model and SODA were calculated (Table 2).

And then, to assess the ability of the coupled ROMS-NPZD model to reproduce realistic chlorophyll patterns and nutrients over the NSCS, the mean surface chlorophyll a and NO_3 concentrations during September to October derived from the NPZD model were compared with the data measured during September to October in 2004, which partly coincided with the summer coastal upwelling in NSCS (Fig. 8). Moreover, satellite-derived high-resolution of surface chlorophyll from the Moderate Resolution Imaging Spectro-radiometer (MODIS) was also compared with the simulated chlorophyll (Fig. 7), which reflects a pretty good match.

Here, a Taylor diagram (Taylor, 2001) was constructed to statistically summarize how closely the simulated results match observations in terms of the standard deviations, the centered root mean square difference and the correlation (Fig. 9).

RMSE and Corrcoef of chlorophyll a and NO_3 concentrations between the model and the measured data were also calculated (Table 2) in order to evaluate the usability of the NPZD model. RMSE value and Corrcoef reflect the forecast accuracy of a model (Park et al., 2009). The smaller RMSE value it is, the higher accuracy of the model results we get. Corrcoef (Ogasawara, 2010) is a kind of value set at $[-1, 1]$, and the closer absolute Corrcoef value approaches to 1, the better-simulated results they would be. Specifically speaking, the simulated results generally well reproduce the observations with the Corrcoef ranging from 0.7 to 0.9, and the normalized standard deviation (NSD) from 0.5 to 0.8 (normalized by the standard deviation of the corresponding observed field, Taylor, 2001). In addition, observing the two line charts (Fig. 10) we can see that the variation trend and the range of concentration are roughly the same.

However, the simulated results of some nearshore stations have relatively large errors, such as station 1 and station 33. After analyzing the causes, we find that these stations located in the Pearl River estuary are affected by the strong Pearl River diluted water, which reflects that there may exist some shortcomings in simulated freshwater flux of the

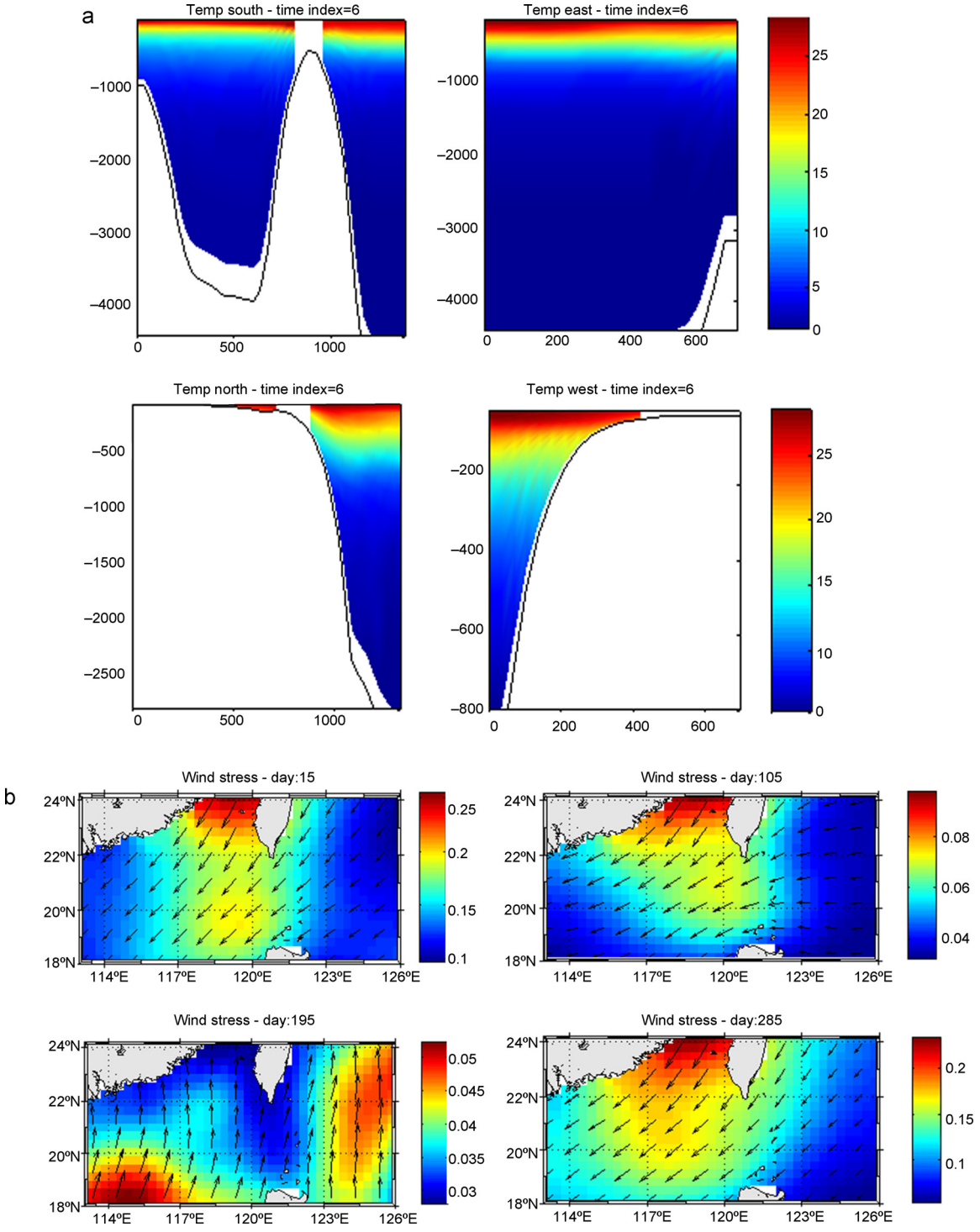

Figure 4 Four different sections of temperature [°C] for initial condition (a), the sections are in the *X*-direction (East—West), the first section is for the southern part of domain and the last one is for the northern part of the domain. The wind stress vectors and wind stress norm (b) obtained from the global atlas of surface marine data at 1/2° at 4 different periods of the year [N m^{-2}].

physical model. On account of the simulated results being climatic, and yet the measured results being discontinuous, interannual variations are allowed; so the differences between them are understandable. Beyond that, the most of the simulated results conform to the measured and satellite data. In sum, this coupled ROMS-NPZD model can be used as the basis of quantitative ecological research. To ensure the accuracy of our study, model results of the third year, which are the most steady simulated results among all the model data, are used to illustrate ecosystem response mechanism.

5. Results description

Coastal upwelling is one of the most important physical processes which has a significant influence on the distribution of nutrients and hence affecting primary production (Krishna, 2008). Upwelling is responsible for transporting higher-salinity and nutrient-rich deeper water to the surface layer. The previous ecological studies on summer upwelling system over the northern continental shelf of SCS were mainly carried out by ship drift data (Cai et al., 2002; Song et al., 2012), and the interannual variation may have a marked impact on the universality of the data. Since this coupled ROMS-NPZD model simulations were climatologically forced runs, the simulated data do not correspond to a specific year.

5.1. Hydrographic conditions response to YDU and QDU

The coastal upwelling in YD and QD are characterized by the flow responding to the southwesterly winds on the shelf. The surface water shows obvious continental shelf upwelling characteristics (Fig. 11), such as low temperature, high salinity in the east of the Leizhou Peninsula (noted as Qiongdong-QD upwelling-QDU), and the inshore areas from the Shantou Coast to the Nanri Islands of Fujian province (noted as Yuedong – YD upwelling – YDU) (Jing et al., 2008). The typical mature upwelling regions of the study areas are characterized by nearshore cold and high-salinity layer, which is surrounded by an offshore warm and low salinity layer, in summer. As the cold upwelling water which is generated near the coast spreads and advects offshore, it pushes warm water far from the coast (Gan et al., 2009a,b). Comparing these two coastal upwelling regions, the salinity of YD is not as high as QD, but it is much higher compared to other coasts around.

The summer coastal upwelling is a regular phenomenon during June to September in NSCS (Yu, 1987). Low temperature in the surface water can be detected clearly in both QD and YD, and it can be about 2–3°C lower than the offshore water (Figs. 12a and b, 13a and b). The variations of temperature in QD (Fig. 12a) and in similar latitudes elsewhere (the region around 113°E) (Fig. 12b) during the simulated three years are showed, respectively. The modeled surface temperature in QD decreases continuously rather than

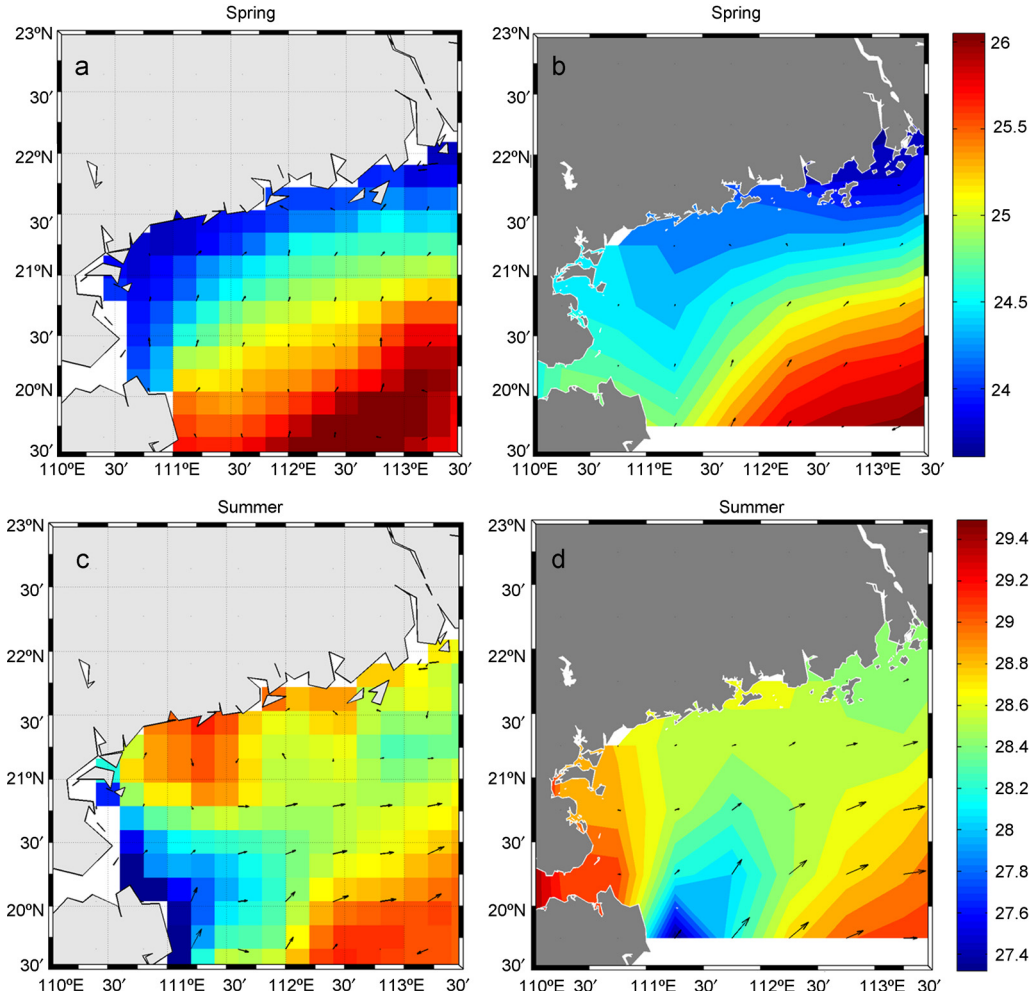

Figure 5 The seasonal changes of the sea surface temperature [°C] and the flow field in the Leizhou Peninsula (QD) simulated by our model (subplots a, c, e, g) and calculated from SODA (subplots b, d, f, h).

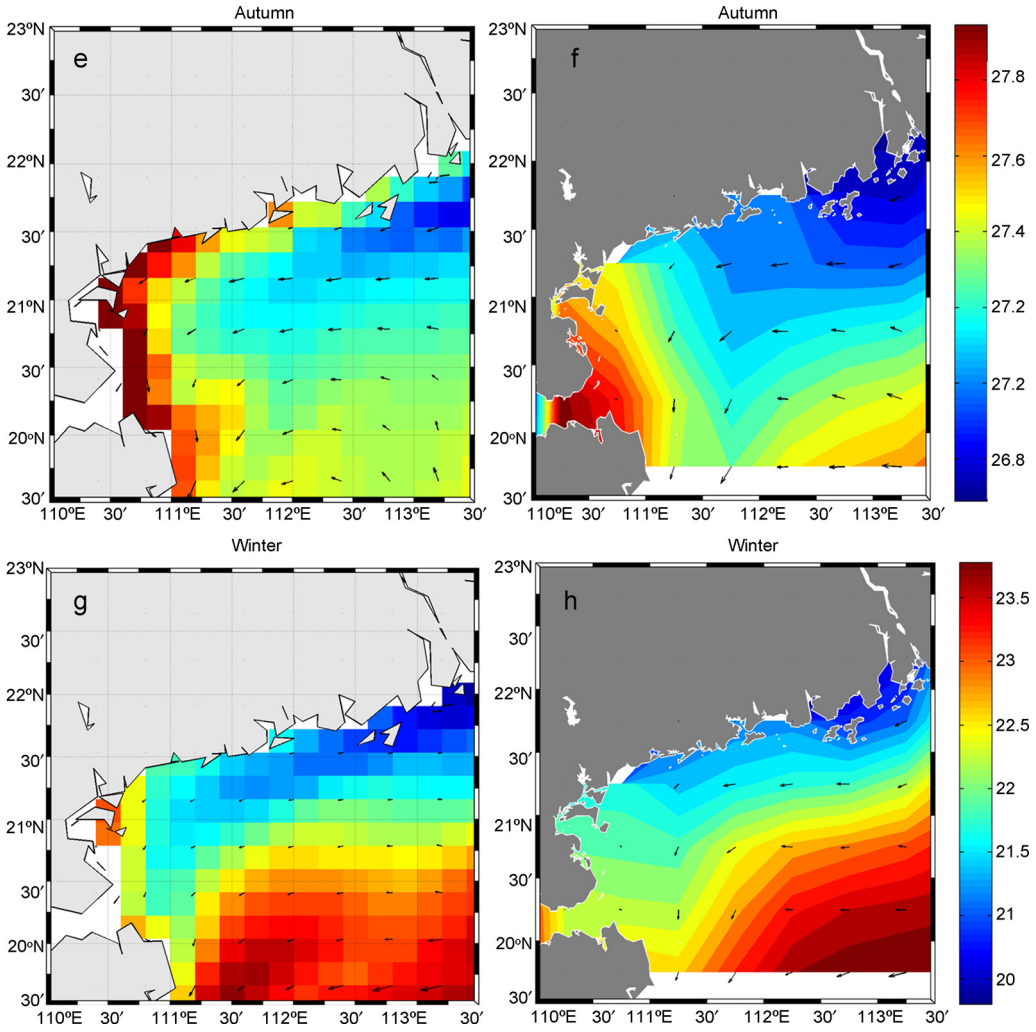

Figure 5. (*Continued*).

increases, and reaches the summer's lowest point in the middle of July, and then rises gradually to the second peak in the middle of September. Moreover, high salinity in the surface water can also be detected in both QD and YD (Figs. 12c and d, 13c and d). Three similar small salinity spikes can be found during every July of the three simulated years (Fig. 12c). The salinity during these periods of time is around 34, just the same as in the results of previous study (Li et al., 2012). However, there are no salinity spikes during the same period of time in the region around 113°E (Fig. 12d), and the salinity (about 32) is significantly lower than in QD.

5.2. Nutrients response to YDU and QDU

The distribution of nutrients in YDU and QDU follows the general pattern of coastal upwelling at other sea areas (Fernandes et al., 2014; Krishna, 2008), which has characteristics of higher concentrations near the subsurface layer of coastal waters and lower concentrations at the surface of offshore waters (Chenillat et al., 2012, 2013). However, the distribution of nutrients in these two regions also has its own characteristics.

It is obvious that the highest NO_3-N concentrations (<0.14 mmol m^{-3}) in the coast around the 115°E (Fig. 14a) are located between −50 m and −60 m water layer, and the NO_3-N concentrations of surface water are very low (<0.08 mmol m^{-3}), which reflects the impacts of stratification existing between the surface and sub-surface layer. And yet, the highest NO_3-N concentrations (>0.17 mmol m^{-3}) in YD appear between −20 m and −40 m water layer, and an enhanced vertical mixing can be found in this water layer (Fig. 14b). Meanwhile, the NO_3-N concentrations of surface water are much higher than in the water layer below −50 m. Compared with the coast around the 115°E, the water layer with the highest NO_3-N concentrations in YD moves up and the mean value of NO_3-N concentrations is much higher (Fig. 14a and b). According to the analysis above, the YDU is responsible for carrying nutrient-rich deeper water toward the surface. However, the NO_3-N concentrations in QD (Fig. 14d) and similar latitudes elsewhere (Fig. 14c) still show the strict vertical stratification, and the NO_3-N concentrations of surface water are much lower (<0.2 mmol m^{-3}). With the increase of water depth, the NO_3-N concentrations

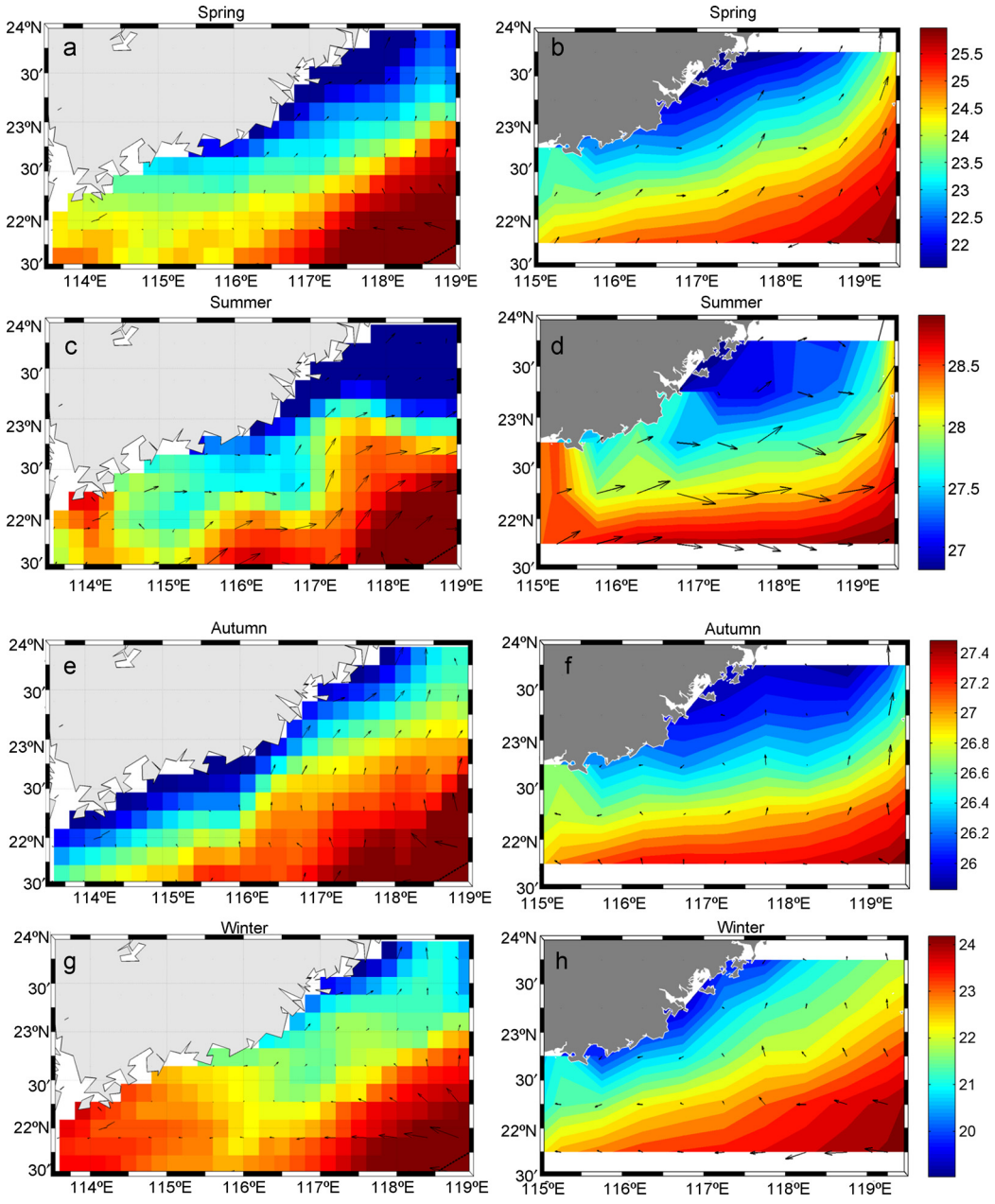

Figure 6 The seasonal changes of the sea surface temperature [°C] and the flow field in the Fujian Province (YD) simulated by our model (subplots (a), (c), (e), (g)) and calculated from SODA (subplots (b), (d), (f), (h)).

increase gradually until the water depth reaches about −70 m (>1.2 mmol m^{-3}).

Although the YDU and QDU are two main coastal upwellings in NSCS, their impacts on the distribution and concentrations of NO_3-N are different. There is an obvious upwelling triggered uplift of NO_3-N in YD, but only a slight upwelling triggered uplift in QD. In addition, the distributions and changes of nutrients may inevitably affect the primary productivity in YD like in the previous studies in other coastal upwelling areas (Hernández-Carrasco et al., 2014).

5.3. Phytoplankton response to YDU and QDU

Phytoplankton is an important bioindicator of chemical and biological modifications in natural ecosystems (Vilhena et al., 2014). It is also an important element of primary production, which is the key basic biological production in marine ecosystems (Song et al., 2010). It has been proposed that in NSCS the distribution of phytoplankton during summer time is closely related to the coupled processes driven by summer southwesterly monsoon induced upwelling (Ning et al., 2004), so are the YUD and QDU.

Table 2 RMSE and Corrcoef of the simulated results.

	Root mean squared error	Correlation coefficient
Chla	0.0989	0.7174
NO_3-N	1.8140	0.8236
u(YD)	0.1922	0.7269
v(YD)	0.0481	0.6507
u(QD)	0.1416	0.6945
v(QD)	0.0796	0.7654

In the middle of July, a great distribution and concentrations differences of phytoplankton exist between YD and the coast around the 115°E (Fig. 15a and b). It is obvious that the highest phytoplankton concentrations are located between −50 m and −70 m water layer (Fig. 15b) in the coast around the 115°E; however, the water column with the highest phytoplankton concentrations move up to −20 m to −40 m in YD (Fig. 15a). Beyond this uplift phenomenon, the phytoplankton concentrations in YD are also a lot higher than in the coast around the 115°E. The NSCS coastal upwelling driven by both upwelling favorable local wind and topography, which affects the distribution of nutrients, then would have an ultimate effect on the phytoplankton growth and standing stock. The YDU is just like a perfect nutrient pump for new production (Wang et al., 2014a,b).

The strongest coastal upwelling with the minimum temperature and the maximum nutrients in NSCS often occurs in the middle of July based on the previous study (Jing et al., 2008). This is the reason why we often use the simulation result of July 16th to illustrate our study. However, the similar rule cannot be applied to phytoplankton. The phytoplankton concentrations in the late July (>0.3 mmol m^{-3}) (Fig. 15c) are higher than in the middle of July (>0.2 mmol m^{-3}) (Fig. 15a). In addition, phytoplankton is advected to almost 30 km off the coast in the late July (Fig. 15c), which is much farther than 15 km in the middle of July (Fig. 15a). The intense YDU occurs in the middle of July, while the phytoplankton blooms in the late of July, which confirms that the maximum phytoplankton do not, in general, coincide with the minimum temperature (Santos et al., 2011; Sawant and Madhupratap, 1996), but are lagged in time, by about 10 days.

Different from YDU, QDU combined with the intensive seasonal thermocline makes the distribution of phytoplankton stratified and the phytoplankton concentrations still very low in the surface layer (Fig. 16a). Comparing with the region around 113°E (Fig. 16b), there is only a slight upwelling triggered uplift of phytoplankton in QD, and the maximum phytoplankton is located within the thermocline coupled to the nutricline. Due to this thermocline induced stratification, the surface productivity in QD may be held back.

5.4. Chlorophyll *a* response to YDU and QDU

At the initial stage, upwelled waters of YDU and QDU are characterized by low temperature, low chlorophyll *a* and

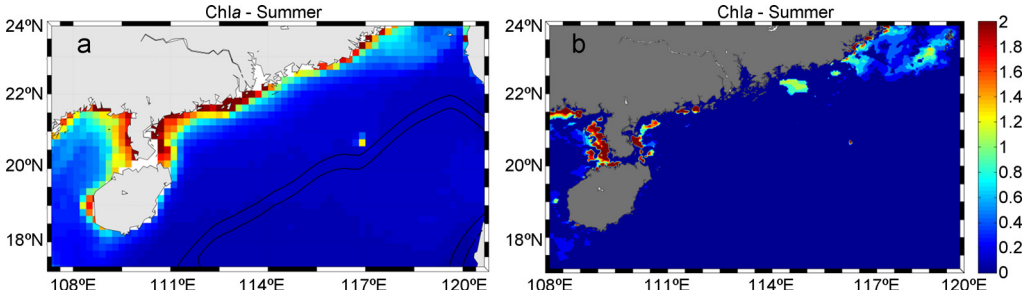

Figure 7 The simulated surface chlorophyll *a* [μg L^{-1}] (a) and satellite-derived high-resolution of surface chlorophyll *a* (b) from the Moderate Resolution Imaging Spectro-radiometer (MODIS).

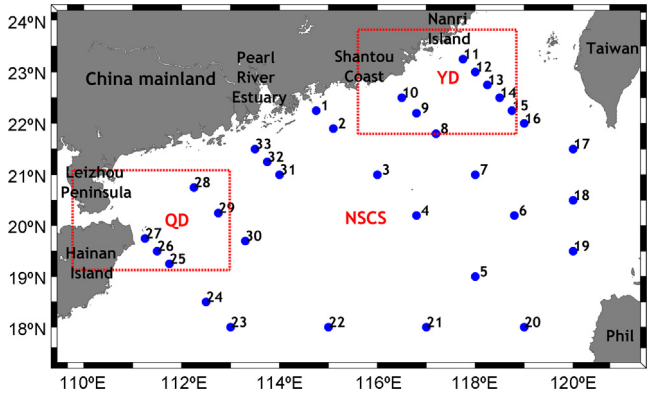

Figure 8 Stations of the measured experiment, which have been used to compare with the simulated results.

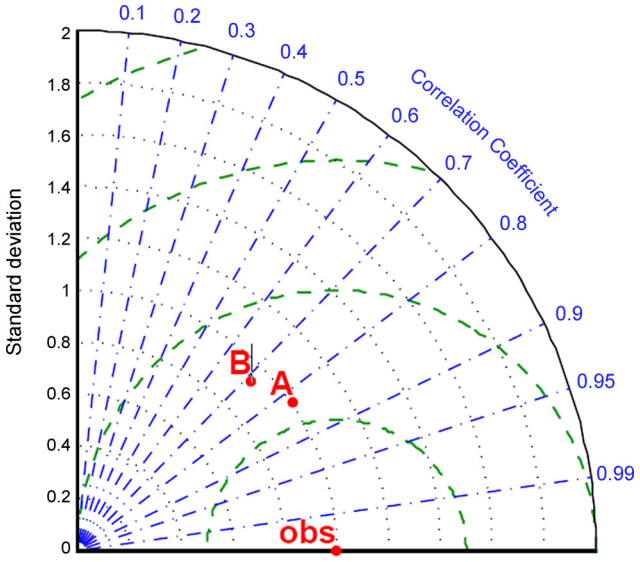

Figure 9 Taylor diagram for model skill assessments. Observations (obs) of stations include sea surface NO_3 (A) and sea surface chlorophyll *a* (B). The radial distance from the origin is proportional to the standard deviation of a pattern. The centered RMS difference between the simulations and obs is proportional to their distance apart (in the same units as the standard deviation). The correlation between the two fields is given by the azimuthal position of the test field.

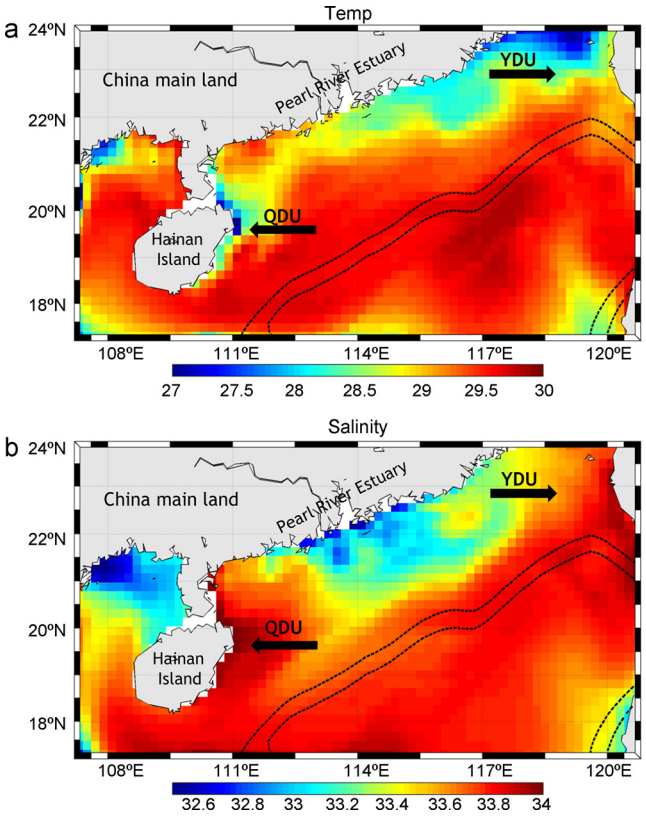

Figure 11 The climatological SST [°C] (a) and surface salinity (b) derived from CARS2009.

high nutrient concentrations (Joint et al., 2001). Afterwards, a fast growth of phytoplankton can take place coincided with the increase of chlorophyll *a* promoting a quick consumption of the available nutrients.

The concentrations of chlorophyll *a* are generally higher toward the inshore areas in YD and QD, and decrease to less than 0.2 ug L^{-1} at the offshore locations (Fig. 17). In YD, the maximum chlorophyll *a* (around 0.45 μg L^{-1}) is observed at −30 m to −20 m water layer in the middle of July (Fig. 17a). Then about 10 days later, the maximum chlorophyll *a* concentrations increase to 0.7 μg L^{-1} recorded at −20 m to lower than −10 m water layer (Fig. 17c). QD presents different distribution characteristics. Higher grazing pressure in the upper layer than at the thermocline may lead to the formation of the subsurface

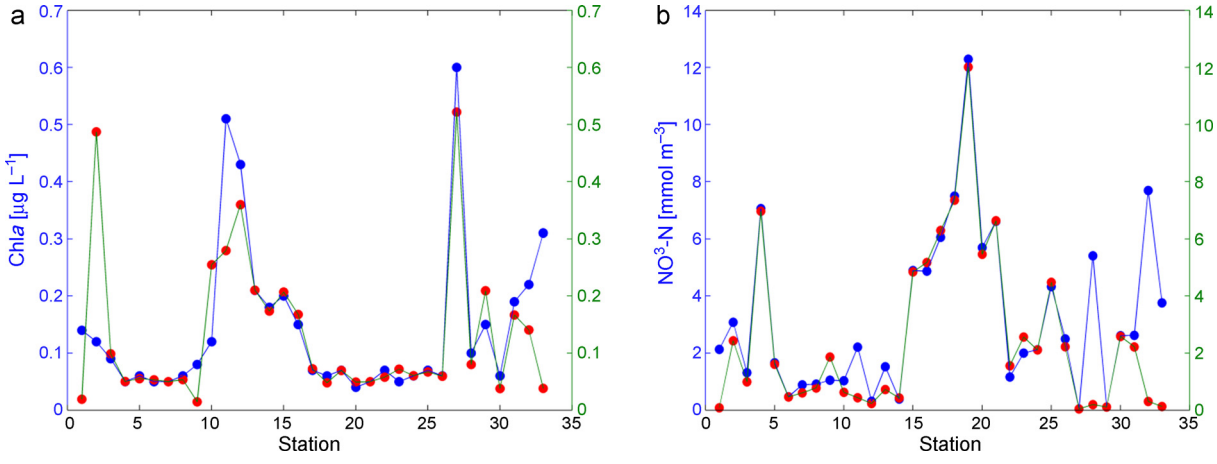

Figure 10 In (a), the blue dot line represents simulated Chl *a* concentrations [μg L^{-1}] and the red dot line represents measured Chl *a* concentrations; in (b), the blue dot line represents simulated NO_3-N concentrations [mmol m^{-3}] and the red dot line represents measured NO_3-N concentrations. (For interpretation of the references to color in this figure legend, the reader is referred to the web version of this article.)

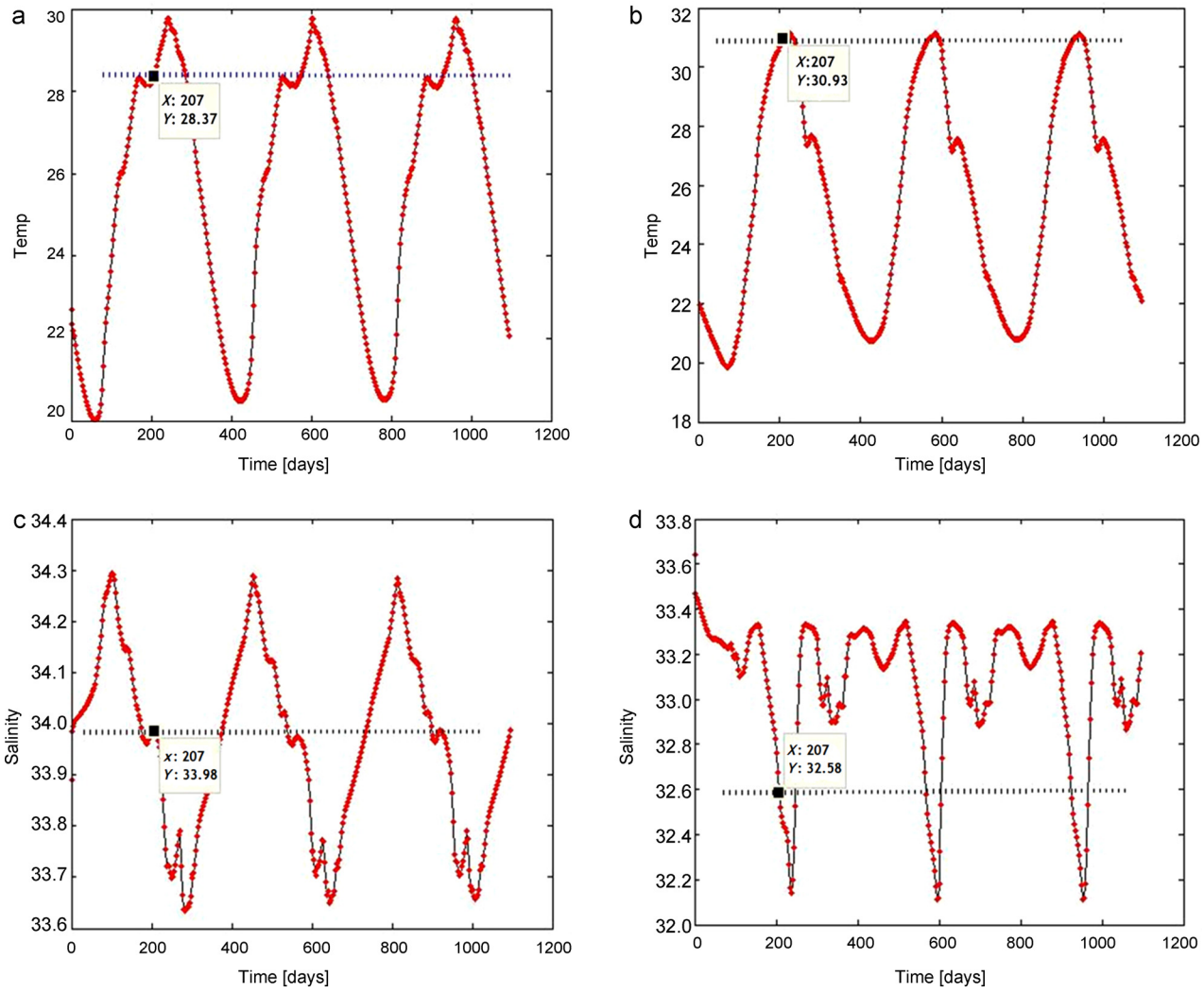

Figure 12 The time series of temperature [°C] in the Leizhou Peninsula (QD – a) and the region around the 113°E (b), the time series of salinity in QD (c) and the region around the 113°E (d).

maximum chlorophyll near the thermocline (Kononen et al., 1998). At QD, the maximum chlorophyll *a* (around 0.5 μg L^{-1}) is observed at −70 m to −60 m water layer in the middle of July (Fig. 17b). Then, about 10 days later, the chlorophyll *a* maxima rise to about 0.65 μg L^{-1} (Fig. 17d). The chlorophyll *a* maxima in YD and QD coincide with the phytoplankton maxima (Figs. 15–17). Similar to the phytoplankton, the maximum chlorophyll *a* does not, in general, coincide with the minimum temperature, which is lagged in time, by about 10 days.

Significant subsurface chlorophyll *a* maximum (SCM) exists in both YD and QD. SCM exists in YD at depth between −40 m and −10 m, and in QD between −70 m and −50 m. The results suggest that the locations of the SCM have close connection with the upward nutrients flux and downward light attenuation. The SCM appears in the same location with the maximum nutrients in the premise that the *PAR* is suitable (Fennel and Boss, 2003). The water layer between −70 m and −50 m in YD, there is not enough nutrients but enough *PAR*, the growth of phytoplankton is limited by nutrients, which leads to the low chlorophyll *a* concentrations. The similar low chlorophyll *a* concentrations phenomenon has also been observed by Lu et al. (2010).

6. Discussion

6.1. Hydrographic differences between YDU and QDU

In this paper, NPZD model rather successfully simulated the ecosystem response to distinctly intensified coastal upwelling over the widened shelf in the NSCS. As seen from model results, the surface water in YD and QD shows obvious continental shelf upwelling characteristics, such as low temperature, high salinity. However, comparing these two coastal upwelling regions, the salinity of YD is not as high as QD because of the effect from the Pearl River diluted

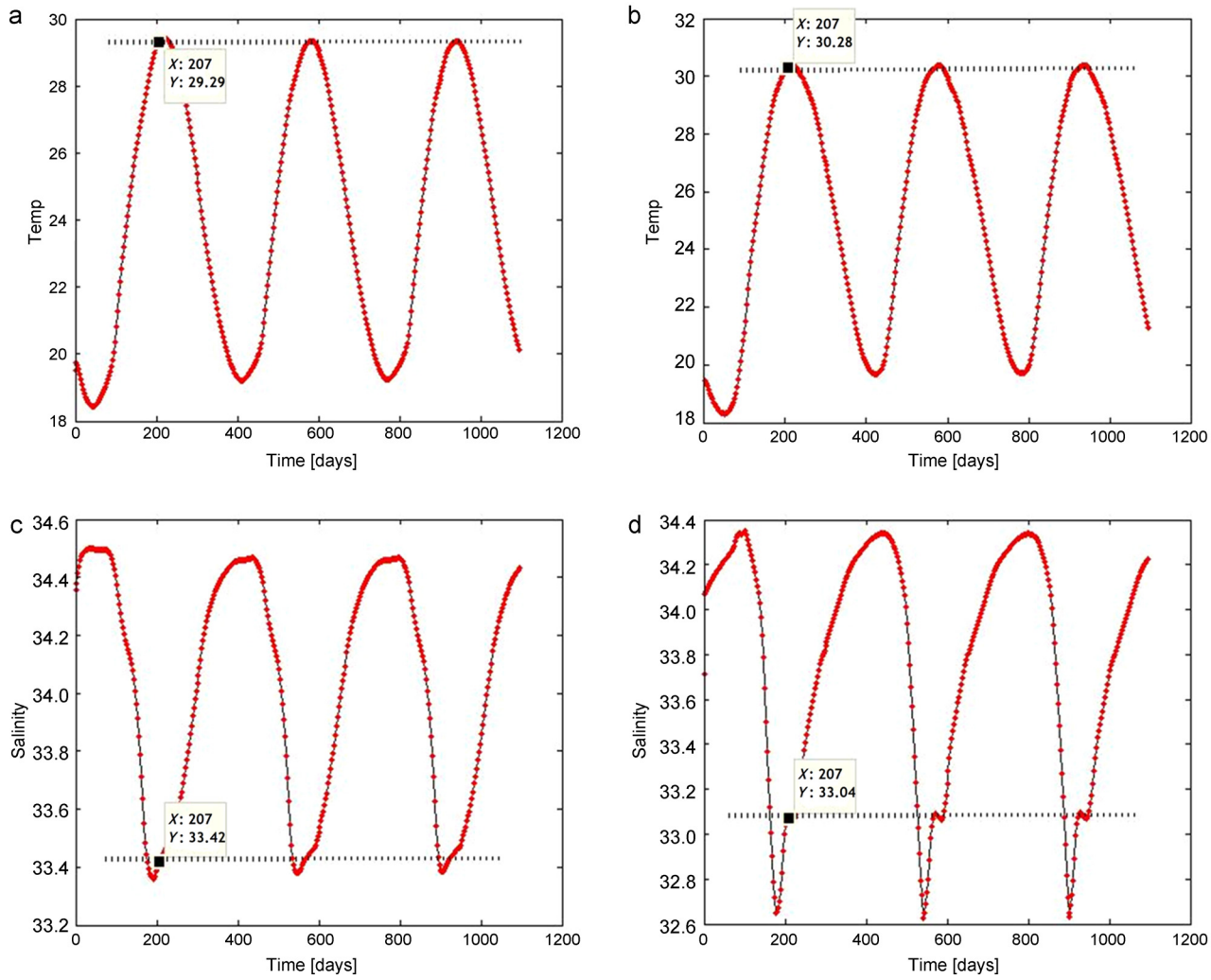

Figure 13 The time series of temperature [°C] in the Fujian Province (YD) (a) and the region around the 115°E (b), the time series of salinity in YD (c) and the region around the 115°E (d).

water (PRDW). The Pearl River is the largest river in south China and has the second largest annual runoff in China. The plume size of PRDW is at maximum in summer, and the southwest monsoon is conducive to the eastward and offshore expansion of the PRDW, which negatively influences the salinity of YD (Dong et al., 2004).

6.2. YDU and QDU acting as a nutrient pump

To comprehend the response of nutrients, the variation trend of nitrate (NO_3-N) was used as representative. According to 'Specification of Oceanographic Investigation', nutrients that include nitrate, nitrite (NO_2), ammonium, phosphate (PO_4-P) and silicate (SiO_3-Si) are often used to represent the main kind of nutrients in the SCS. Nevertheless, only NO_3-N has been simulated in our model study. The principal component analysis (PCA) was utilized to analyze nutrients in NSCS. Based on this former study, NO_3-N has positive correlations with NH_4-N and SiO_3-Si (Wu and Wang, 2007). Hence, NO_3-N has a certain degree of representativeness. In our study, there is an obvious upwelling triggered uplift of NO_3-N in YD, but only a slight upwelling triggered uplift in QD. Not only taking into account the summer coastal seasonal upwelling in NSCS, June to August is also a period of time, during which the most intensive thermocline happens in NSCS (Li and Jian, 2001). In some shallow waters of SCS, there exists the radiation-type seasonal thermocline, which is affected by gross radiation intensity and Ekman pumping (Liu et al., 2001). During every year from March to August, the seasonal thermocline appears in the southeast of the Hainan Island and the northwest of the Taiwan Island, which is almost in the same spot as QD and YD. From March to May is a sharp period of the thermocline in these two regions, and from June to August is the strongest period (Fan et al., 2014). The difference is that the seasonal thermocline in the southeast of Hainan Island is much stronger than in the northwest of Taiwan Island. At QD, prominent signatures providing evidence for the prevalence of upwelling are

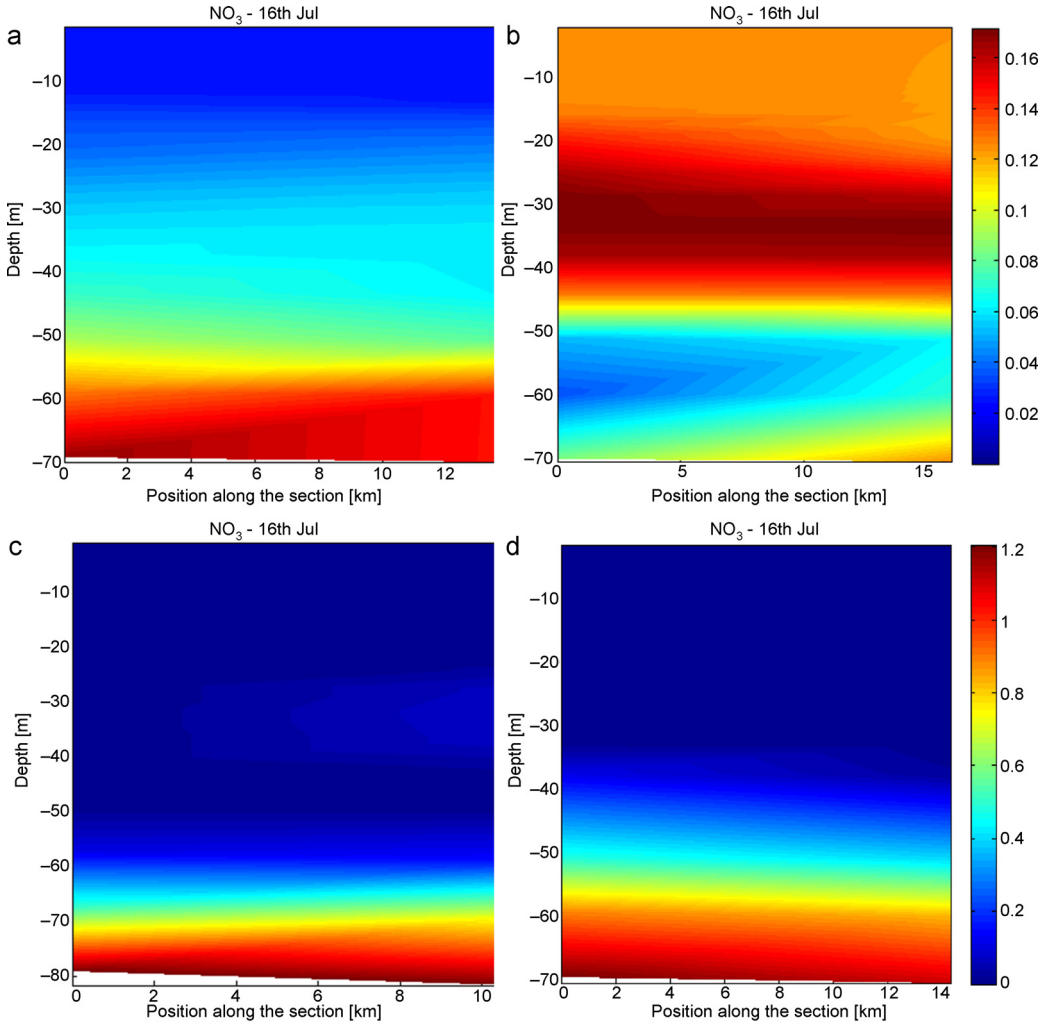

Figure 14 The vertical distribution of NO_3-N [mmol m^{-3}] with "interannual timescale" on the caption, "offshore distance" on the horizontal axis, and "depth" on the vertical axis. Subplots (a) represents the simulated results of the region around the 1158E; subplots (b) represents the simulated results of the Fujian Province (YD); subplots (c) represents the simulated results of the region around the 1138E; subplots (d) represents the model results of the Leizhou Peninsula (QD).

not only based on the sea surface temperature anomaly but also on the notable shoaling of the thermocline. The thermocline in the southeast of Hainan Island is too strong to break into surface by the QDU, hence there is only a slight upwelling triggered uplift of NO_3-N in QD. This thermocline leads to the shortage of nutrients in surface water, and may hold back the productivity in QD. Besides the impact of the thermocline, the water current and transport through Qiongzhou strait is very complicated in summer (Fig. 18) (Wang et al., 2014a,b), which also affects the variation trend of nutrients in QD.

6.3. Delay effects of phytoplankton and chlorophyll *a* in YD

The maximum amount of phytoplankton and chlorophyll *a* does not, in general, coincide with the minimum temperature and maximum nutrients (Santos et al., 2011), but is lagged in time, by nearly 10 days. In our study, the maximum amount appears (in July 28th) with lower upward water velocities (Fig. 19). This phenomenon is common in many upwelling systems in the world (Muller-Karger et al., 2001; Yokomizo et al., 2010) and it is related to the reaction time needed by phytoplankton to react to the sudden increase in nutrient concentrations, which can be about 8–10 days (MacIsaac et al., 1985). Following the previous study (Huete-Ortega et al., 2010), when upward water velocities are highest, together with relatively strong turbulence, they prevent the accumulation of large amounts of phytoplankton; for it takes time for phytoplankton communities to adjust to the new nutrients condition. On the other hand, the upwelling relaxation combining with increased water-column stability and reduced dispersion create appropriate conditions for the onset of the phytoplankton blooms (Lopes et al., 2014). In addition, the development rate

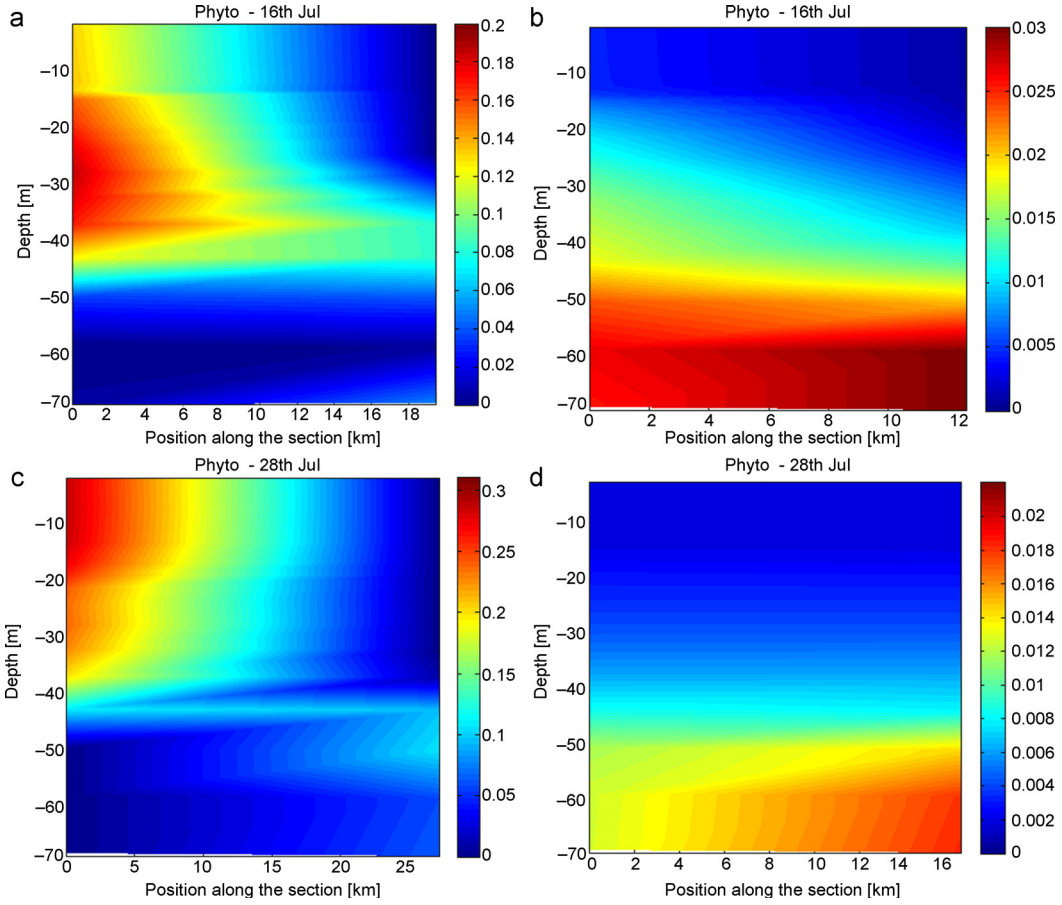

Figure 15 The vertical distribution of phytoplankton [mmol m^{-3}] with an "interannual timescale" on the caption, "offshore distance" on the horizontal axis, and "depth" on the vertical axis. Subplots (a) and (c) represent the model results of the Fujian Province (YD) in July 16 and July 28; subplots (b) and (d) represent the model results of the region around the 1158E in July 16 and July 28.

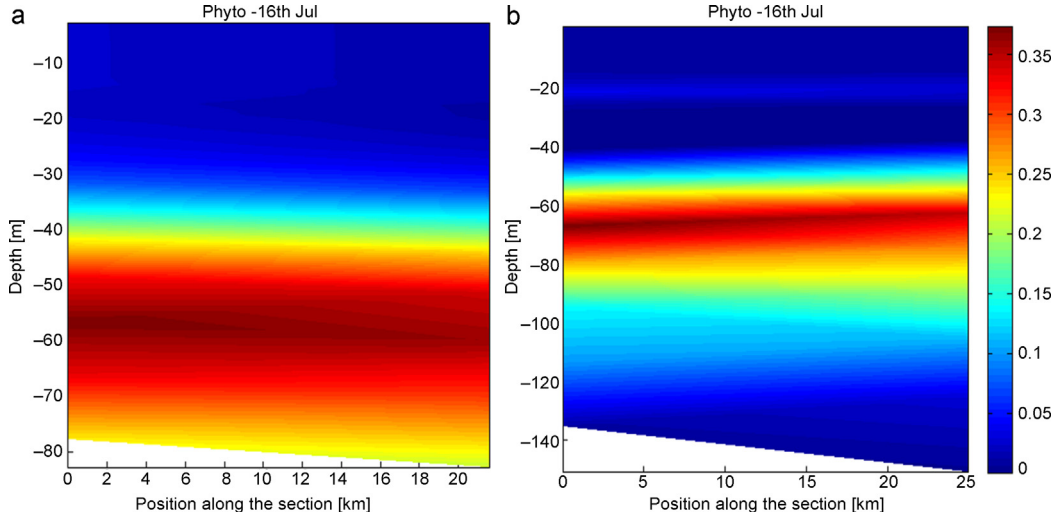

Figure 16 The vertical distribution of phytoplankton [mmol m^{-3}] with an "interannual timescale" on the caption, "offshore distance" on the horizontal axis, and "depth" on the vertical axis. Subplot (a) represents the model results of the Leizhou Peninsula (QD) in July 16, and subplot (b) presents the model results of the region around the 1138E in July 16.

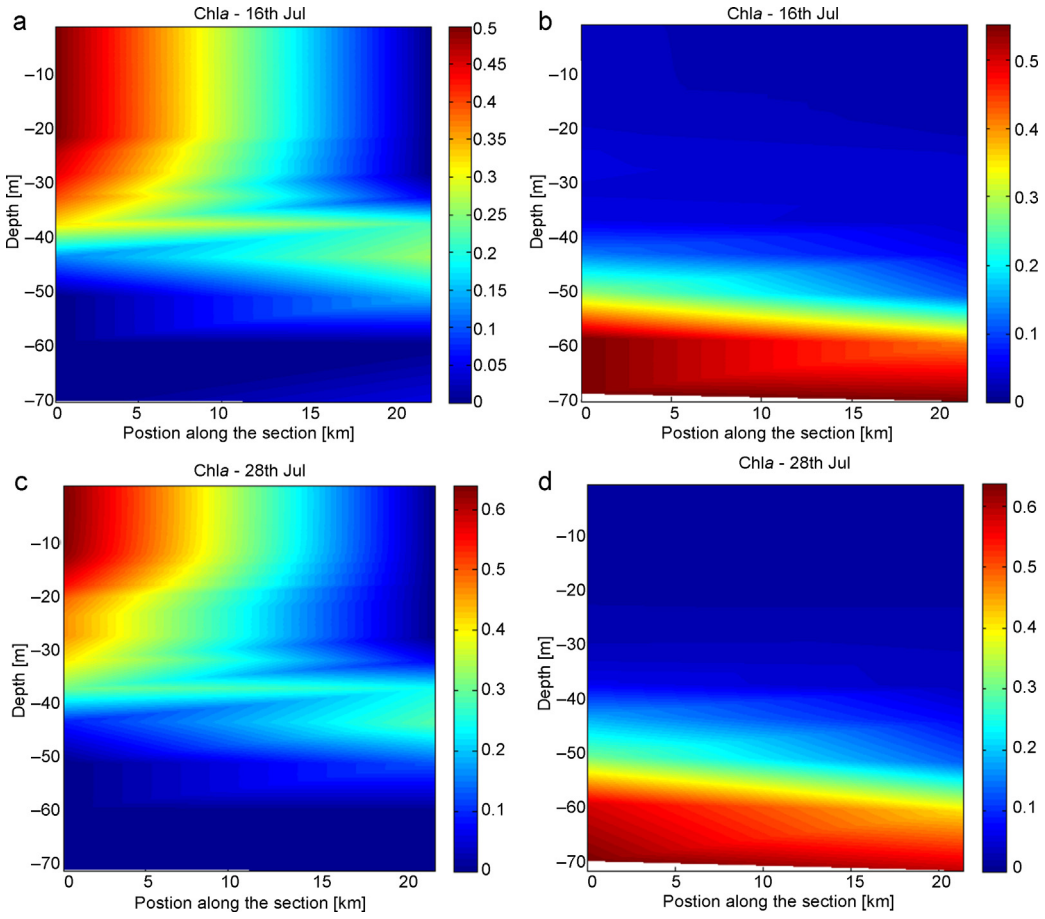

Figure 17 The vertical distribution of chlorophyll *a* [μg L^{-1}] with an "interannual timescale" on the caption, "offshore distance" on the horizontal axis, and "depth" on the vertical axis. Subplots (a) and (b) represent the model results of the Fujian Province (YD) and the Leizhou Peninsula (QD) in July 16; subplots (c) and (d) represent the model results of YD and QD in July 28.

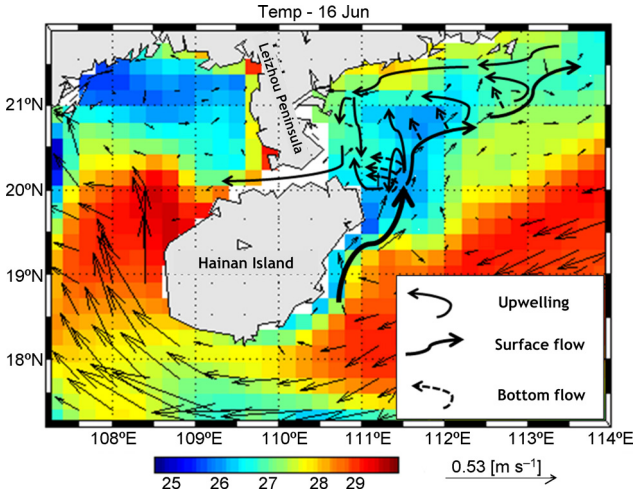

Figure 18 The water current, and its transport in the Leizhou Peninsula (QD).

of phytoplankton is closely related to the shelf width. The development rate changes from very wide (fast) to narrow (slow) (Botsford et al., 2003). The widened shelf off Shanwei and on the western flank of the Taiwan Banks intensifies the bottom friction, which is a key factor for topographically induced upwelling and also has a positive correlation to the development of phytoplankton. The phytoplankton production increases with lower wind strength, and in proportion to upwelled volume, but eventually begin to decrease as losses increase off the shelf (compared with Fig. 15c, Fig. 20 shows a remarkable decrease). Moreover, high offshore velocities on the seaward side advect the upwelling water off the coast, which leads to the strong phytoplankton concentrations at about −10 m to −40 m water layer extending seaward from the inner shelf to about 30 km into outer shelf (Fig. 15c).

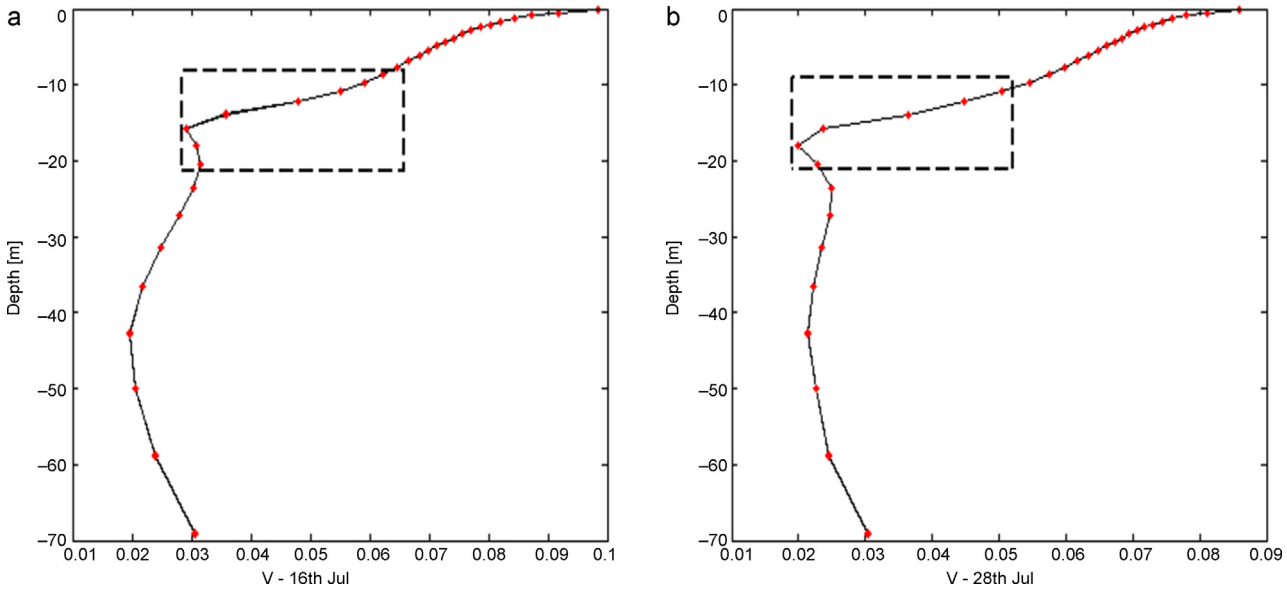

Figure 19 The upward water velocities [m s^{-1}] in the Fujian Province (YD). Subplot (a) represents the model results of YD in July 16, and subplot (b) represents the model results of YD in July 28.

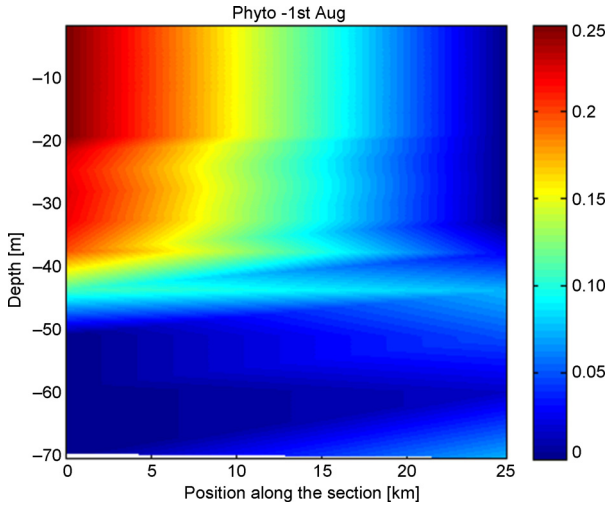

Figure 20 The vertical distribution of phytoplankton [mmol m^{-3}] of the Fujian Province (YD) in August 1st, with an "interannual timescale" on the caption, "offshore distance" on the horizontal axis, and "depth" on the vertical axis.

7. Conclusion

The coastal upwelling blooms common to the NSCS are captured by the model (ROMS-NPZD). Although in a simple framework, the results from our coupled biological-physical model are in qualitative agreement with the general characteristics of the NSCS coastal upwelling system. Based on our ecological model study, the ecosystem response to the summer coastal upwelling in NSCS can be summarized as follows.

YDU and QDU are physical processes which occur in sequential stages: (1) the first stage can be defined by the offshore transport of surface water and its replacement by cold, nutrient rich sub-surface water; (2) the second stage is the productive phase wherein an increase in phytoplankton and chlorophyll standing stock can be found.

During summer, YD and QD are characterized by nearshore cold and high salinity layer surrounded by an offshore warm and low salinity layer. The water temperature at YD and QD can be about 2—3°C lower than the offshore water, and the salinity is around 34 which is much higher than 32 in the offshore water. At YD and QD, the nutrients in the subsurface water layer also display high concentrations. There is an obvious upwelling triggered uplift of NO_3-N in YD. However, due to the impact of the intensive seasonal thermocline and the complex currents system, QD only display a slight upwelling triggered uplift of NO_3-N.

Similar to NO_3-N, an obvious upwelling triggered uplift of phytoplankton can also be found in YD. Unlike NO_3-N, the maximum phytoplankton do not, in general, coincide with the intense YDU, but is lagged in time, by about 10 days. Moreover, high offshore velocities on the seaward side advect the upwelled water off the coast, which leads to the strong phytoplankton concentrations at about −30 m to −40 m water layer extending seaward from the inner shelf to about 30 km into outer shelf. Nevertheless, being affected by the intensive seasonal thermocline, maximum phytoplankton in QD is located within the thermocline, coupled to the nutricline. The chlorophyll *a* concentrations and distribution in YD and QD are exactly similar to phytoplankton. The chlorophyll *a* maxima at YD and QD coincide with the phytoplankton maxima, and hence the maximum chlorophyll *a* does not, in general, coincide with the minimum temperature; but are lagged in time, by about 10 days.

It should be noted that the summer coastal upwelling system in the NSCS is too complicated to understand it fully. According to its impacts on the temperature, salinity, nutrients, phytoplankton and chlorophyll *a* presented in this paper, the summer coastal upwelling system must have a

significant effect on the distribution of marine organisms and the protection of NSCS coastal environment.

Acknowledgements

This research was supported by the Strategic Priority Research Program of the Chinese Academy of Sciences (XDA10020225), the research project of State Key Laboratory of Tropical Oceanography, the National Natural Science Foundation of China (41430966), National Key Research and Development Program of China (2017FY100700) and the Projects of Guangzhou Science and Technology (201504010006). We deeply appreciate the journal editors and the two anonymous reviewers for their constructive comments and suggestion.

References

Botsford, L.W., Lawrence, C.A., Dever, E.P., Hastings, A., Largier, J., 2003. Wind strength and biological productivity in upwelling systems: an idealized study. Fish. Oceanogr. 12 (4–5), 245–259, http://dx.doi.org/10.1046/j.1365-2419.2003.00265.x.

Cai, P.H., Huang, Y.P., Chen, M., Guo, L.D., Liu, G.S., Qiu, Y.S., 2002. New production based on Ra-228-derived nutrient budgets and thorium-estimated POC export at the intercalibration station in the South China Sea. Deep-Sea Res. Pt. I 49 (1), 53–66, http://dx.doi.org/10.1016/S0967-0637(01)00040-1.

Casey, K.S., Cornillon, P., 1999. A comparison of satellite and in situ-based sea surface temperature climatologies. J. Clim. 12 (6), 1848–1863, http://dx.doi.org/10.1175/1520-0442(1999)012<1848:ACOSAI>2.0.CO;2.

Chelton, D.B., DeSzoeke, R.A., Schlax, M.G., El Naggar, K., Siwertz, N., 1998. Geographical variability of the first baroclinic Rossby radius of deformation. J. Phys. Oceanogr. 28 (3), 433–460, http://dx.doi.org/10.1175/1520-0485(1998)028<0433:GVOTFB>2.0.CO;2.

Chen, C.C., Shiah, F.K., Chung, S.W., Liu, K.K., 2006. Winter phytoplankton blooms in the shallow mixed layer of the South China Sea enhanced by upwelling. J. Mar. Syst. 59 (1–2), 97–110, http://dx.doi.org/10.1016/j.jmarsys.2005.09.002.

Chenillat, F., Riviere, P., Capet, X., Di Lorenzo, E., Blanke, B., 2012. North Pacific Gyre Oscillation modulates seasonal timing and ecosystem functioning in the California Current upwelling system. Geophys. Res. Lett. 39 (1), L15606, 6 pp., http://dx.doi.org/10.1029/2011GL049966.

Chenillat, F., Riviere, P., Capet, X., Franks, P.J.S., Blanke, B., 2013. California coastal upwelling onset variability: cross-shore and bottom-up propagation in the planktonic ecosystem. PLOS ONE 8 (5), e66281, 15 pp., http://dx.doi.org/10.1371/journal.pone.0062281.

Cropper, W.P., DiResta, D., 1999. Simulation of a Biscayne Bay, Florida commercial sponge population: effects of harvesting after Hurricane Andrew. Ecol. Model. 118 (1), 1–15, http://dx.doi.org/10.1016/S0304-3800(99)00039-3.

Davenport, E.D., Fan, C., Govoni, J.J., Anderson, J., 2012. Description and application of a NPZD Model to forecast hurricane impacts to secondary production in coastal ecosystems. Proc. Environ. Sci. 13, 1569–1584, http://dx.doi.org/10.1016/j.proenv.2012.01.149.

Dong, L.X., Sun, J.L., Wong, L.A., Cao, Z.Y., Chen, J.C., 2004. Seasonal variation and dynamics of the Pearl River plume. Cont. Shelf. Res. 24 (16), 1761–1777, http://dx.doi.org/10.1016/j.csr.2004.06.006.

Ehlert, C., Grasse, P., Frank, M., 2013. Changes in silicate utilisation and upwelling intensity off Peru since the Last Glacial Maximum – insights from silicon and neodymium isotopes. Quater. Sci. Rev. 72 (4), 18–35, http://dx.doi.org/10.1016/j.quascirev.2013.04.013.

Fan, W., Song, J.B., Li, S., 2014. A numerical study on seasonal variations of the thermocline in the South China Sea based on the ROMS. Acta Oceanol. Sin. 33 (7), 56–64, http://dx.doi.org/10.1007/s13131-014-0504-8.

Fennel, K., Boss, E., 2003. Subsurface maxima of phytoplankton and chlorophyll: steadystate solutions from a simple model. Limnol. Oceanogr. 48 (4), 1521–1534, http://dx.doi.org/10.4319/lo.2003.48.4.1521.

Fasham, M.J.R., Ducklow, H.W., Mckelvie, S.M., 1990. A nitrogen-based model of plankton in the oceanic mixed layer. J. Mar. Res. 48 (3), 591–639, http://dx.doi.org/10.1357/002224090784984678.

Fernandes, S.O., Halarnekar, R., Malik, A., Vijayan, V., Kumari, R., Jineesh, V.K., Gauns, M.U., Nair, S., LokaBharathi, P.A., 2014. Nitrate reducing activity pervades surface waters during upwelling. J. Mar. Syst. 137 (3), 35–46, http://dx.doi.org/10.1016/j.jmarsys.2014.04.011.

Freon, P., Barange, M., Aristegui, J., 2009. Eastern boundary upwelling ecosystems: integrative and comparative approaches preface. Prog. Oceanogr. 83 (1–4), 1–15, http://dx.doi.org/10.1016/j.pocean.2009.08.001.

Gan, J.P., Cheung, A., Guo, X.G., Li, L., 2009a. Intensified upwelling over a widened shelf in the northeastern South China Sea. J. Geophys. Res. 114 (C9), 2157–2165, http://dx.doi.org/10.1029/2007JC004660.

Gan, J.P., Lu, Z.M., Dai, M.H., Cheung, A.Y.Y., Liu, H.B., Paul, H., 2009b. Biological response to intensified upwelling and a river plume in the northeastern South China Sea: a modeling study. J. Geophys. Res. 115 (C9), 292–295, http://dx.doi.org/10.1029/2009JC005569.

González-Gil, R., González Taboada, F., Höfer, J., Anadón, R., 2015. Winter mixing and coastal upwelling drive long-term changes in zooplankton in the Bay of Biscay (1993–2010). J. Plankton Res. 37 (2), 337–351, http://dx.doi.org/10.1093/plankt/fbv001.

Heinle, A., Slawig, T., 2013. Internal dynamics of NPZD type ecosystem models. Ecol. Model. 254, 33–42, http://dx.doi.org/10.1016/j.ecolmodel.2013.01.012.

Hernández-Carrasco, I., Rossi, V., Hernández-García, E., Garcon, V., López, C., 2014. The reduction of plankton biomass induced by mesoscale stirring: a modeling study in the Benguela upwelling. Deep-Sea Res. Pt. I 839 (1), 65–80, http://dx.doi.org/10.1016/j.dsr.2013.09.003.

Huete-Ortega, M., Marañón, E., Varela, M., Bode, A., 2010. General patterns in the size scaling of phytoplankton abundance in coastal waters during a 10-year time series. J. Plankton Res. 32 (1), 1–14, http://dx.doi.org/10.1093/plankt/fbp104.

Jing, Z.Y., Qi, Y.Q., Hua, Z.L., 2008. Numerical study on summer upwelling over northern continental shelf of South China Sea. J. Trop. Oceanogr. 30 (6), 1068–1081, (in Chinese).

Joint, I., Inall, M., Torres, R., Figueiras, F.G., Alvarez-Salgado, X.A., Andrew, P.R., Woodward, E.M.S., 2001. Two Lagrangian experiments in the Iberian Upwelling System: tracking an upwelling event and an off-shore filament. Prog. Oceanogr. 51 (2–4), 221–248, http://dx.doi.org/10.1016/S0079-6611(01)00068-4.

Kononen, K., Hallfors, S., Kokkonen, M., Kuosa, H., Laanemets, J., Pavelson, J., Autio, R., 1998. Development of a subsurface chlorophyll maximum at the entrance to the Gulf of Finland, Baltic Sea. Limnol. Oceanogr. 43 (6), 1089–1106, http://dx.doi.org/10.4319/lo.1998.43.6.1089.

Krishna, K.M., 2008. Coastal upwelling along the southwest coast of India – ENSO modulation. Ann. Geophys. 26 (6), 123–134, http://dx.doi.org/10.5194/angeo-26-1331-2008.

Li, B.H., Jian, Z.M., 2001. Evolution of planktonic foraminifera and thermocline in the southern South China Sea since 12 Ma (ODP-184, Site 1143). Sci. China Ser. D – Earth Sci. 44 (10), 889–896, http://dx.doi.org/10.1007/BF02907080.

Li, R.H., Liu, S.M., Li, Y.W., Zhang, G.L., Ren, J.L., Zhang, J., 2014. Nutrient dynamics in tropical rivers, lagoons, and coastal ecosystems of eastern Hainan Island, South China Sea. Biogeosciences 11 (2), 481–506, http://dx.doi.org/10.5194/bg-11-481-2014.

Li, Y.N., Peng, S.Q., Yang, W., Wang, D.X., 2012. Numerical simulation of the structure and variation of upwelling off the east coast of Hainan Island using QuikSCAT winds. Chin. J. Oceanol. Limnol. 30 (6), 1068–1081, http://dx.doi.org/10.1007/s00343-012-1275-8.

Li, Q.P., Wang, Y.J., Dong, Y., Gan, J.P., 2015. Modeling long-term change of planktonic ecosystems in the northern South China Sea and the upstream Kuroshio Current. J. Geophys. Res. 120 (6), 3913–3936, http://dx.doi.org/10.1002/2014JC010609.

Liu, Q.Y., Jia, Y.L., Liu, P.H., Wang, Q., Chu, P.C., 2001. Seasonal and intraseasonal thermocline variability in the Central South China Sea. Geophys. Res. Lett. 28 (23), 4467–4470, http://dx.doi.org/10.1029/2001GL013185.

Lopes, J.F., Ferreira, J.A., Cardoso, A.C., Rocha, A.C., 2014. Variability of temperature and chlorophyll of the Iberian Peninsula near coastal ecosystem during an upwelling event for the present climate and a future climate scenario. J. Mar. Syst. 129 (1), 271–288, http://dx.doi.org/10.1016/j.jmarsys.2013.07.002.

Lu, Z.M., Gan, J.P., Dai, M.H., Cheung, A.Y.Y., 2010. The influence of coastal upwelling and a river plume on the subsurface chlorophyll maximum over the shelf of the northeastern South China Sea. J. Mar. Syst. 82 (1–2), 35–46, http://dx.doi.org/10.1016/j.jmarsys.2010.03.002.

MacIsaac, J.J., Dugdale, R.C., Barber, R.T., Blasco, D., Packard, T.T., 1985. Primary production cycle in an upwelling center. Deep-Sea Res. Pt. I 32 (5), 503–529, http://dx.doi.org/10.1016/0198-0149(85)90042-1.

Morton, B., Blackmore, G., 2000. South China Sea. Mar. Pollut. Bull. 42 (12), 1236–1263, http://dx.doi.org/10.1016/S0025-326X(01)00240-5.

Muller-Karger, F., Varela, R., Thunell, R., Scranton, M., Bohrer, R., Taylor, G., Capelo, J., Astor, Y., Tappa, E., Ho, T.Y., Walsh, J.J., 2001. Annual cycle of primary production in the Cariaco Basin: response to upwelling and implications for vertical export. J. Geophys. Res. 106 (C3), 4527–4542, http://dx.doi.org/10.1029/1999JC000291.

Ning, X., Chai, F., Xue, H., Cai, Y., Liu, C., Shi, J., 2004. Physical–biological oceanographic coupling influencing phytoplankton and primary production in the South China Sea. J. Geophys. Res. 109 (C10), 215–255, http://dx.doi.org/10.1029/2004JC002365.

Ogasawara, H., 2010. Accurate distribution and its asymptotic expansion for the tetrachoric correlation coefficient. J. Multivariate-Anal. 101 (4), 936–948, http://dx.doi.org/10.1016/j.jmva.2009.12.011.

Park, T.Y., Jang, I.S., Ha, Y.H., 2009. Banding artifact reduction with interweaving dot dispersion based on probability model and human visual system weighted root mean squared error in blue noise multilevel dithering. J. Imaging Sci. Technol. 53 (6), 60504-1–60504-13, http://dx.doi.org/10.2352/J.ImagingSci.Technol.2009.53.6.060504.

Penven, P., Debreu, L., Marchesiello, P., McWilliams, J.C., 2006. Evaluation and application of the ROMS 1-way embedding procedure to the central california upwelling system. Ocean Model. 12 (1–2), 157–187, http://dx.doi.org/10.1016/j.ocemod.2005.05.002.

Powell, T.M., Lewis, C.V.W., Curchitser, E.N., Haidvogel, D.B., Hermann, A.J., Dobbins, E.L., 2006. Results from a three-dimensional, nested biological-physical model of the California Current System and comparisons with statistics from satellite imagery. J. Geophys. Res. 111 (C7), 520–522, http://dx.doi.org/10.1029/2004JC002506.

Prego, R., Guzmán-Zuñiga, D., Varela, M., de Castro, M., Gómez-Gesteira, M., 2007. Consequences of winter upwelling events on biogeochemical and phytoplankton patterns in a western Galician ria (NW Iberian peninsula). Estuar. Coast. Shelf Sci. 73 (3–4), 409–422, http://dx.doi.org/10.1016/j.ecss.2007.02.004.

Riley, G.A., Stommel, H., 1949. Quantitative ecology of the plankton of the Western North Atlantic. Bull. Bingham Oceanogr. Collect. 12 (3), 1–169.

Ruzicka, J.J., Brink, K.H., Gifford, D.J., Bahr, F., 2016. A physically coupled end-to-end model platform for coastal ecosystems: simulating the effects of climate change and changing upwelling characteristics on the Northern California Current ecosystem. Ecol. Model. 331, 86–99, http://dx.doi.org/10.1016/j.ecolmodel.2016.01.018.

Santos, F., Gesteira, M.G., Decastro, M., 2011. Coastal and oceanic SST variability along the western Iberian Peninsula. Cont. Shelf. Res. 31 (19), 2012–2017, http://dx.doi.org/10.1016/j.csr.2011.10.005.

Sawant, S.S., Madhupratap, M., 1996. Seasonality and composition of phytoplankton in the Arabian Sea. Curr. Sci. India 71 (11), 869–873.

Shchepetkin, A.F., McWilliams, J.C., 2005. The regional oceanic modeling system (ROMS): a split-explicit, free-surface, topography-following-coordinate oceanic model. Ocean Model. 9 (4), 347–403, http://dx.doi.org/10.1016/j.ocemod.2004.08.002.

Shchepetkin, A.F., McWilliams, J.C., 1998. Quasi-monotone advection schemes based on explicit locally adaptive dissipation. Mon. Weather Rev. 126 (6), 1541–1580, http://dx.doi.org/10.1175/1520-0493(1998)126<1541:QMASBO>2.0.CO;2.

Song, X.Y., Lai, Z.G., Ji, R.B., Chen, C.S., Zhang, J.L., Huang, L.M., Yin, J.Q., Wang, Y.S., Lian, S.M., Zhu, X.M., 2012. Summertime primary production in northwest South China Sea: interaction of coastal eddy, upwelling and biological processes. Cont. Shelf. Res. 48 (1), 110–121, http://dx.doi.org/10.1016/j.csr.2012.07.016.

Song, X.Y., Liu, H., Huang, L., 2010. Distribution characteristics of basic biological production and its influencing factors in the northern South China Sea in summer. Acta Ecol. Sin. 30 (23), 6409–6417, http://dx.doi.org/1000-0933(2010)30:23<6409:NHBBXJ>2.0.TX;2-G.

Taylor, K.E., 2001. Summarizing multiple aspects of model performance in a single diagram. J. Geophys. Res. 106 (D7), 7183–7192, http://dx.doi.org/10.1029/2000JD900719.

Turner, J.T., Tester, P.A., 1997. Toxic marine phytoplankton, zooplankton grazers, and pelagic food webs. Limnol. Oceanogr. 42 (5), 1203–1214, http://dx.doi.org/10.4319/lo.1997.42.5_part_2.1203.

Vilhena, M.D.S.P., Costa, M.L.D., Berrêdo, J.F., Paiva, R.S., Almeida, P.D., 2014. Chemical composition of phytoplankton from the estuaries of Eastern Amazonia. Acta Amazon. 44 (4), 513–526, http://dx.doi.org/10.1590/1809-4392201305244.

Wang, Y.S., 2013. Quantitative Marine Ecology. Sci. Press, Beijing, 328–334.

Wang, D.X., Shu, Y.Q., Xue, H.J., Hu, J.Y., Chen, J., Zhuang, W., Zu, T.T., Xu, J.D., 2014a. Relative contributions of local wind and topography to the coastal upwelling intensity in the northern South China Sea. J. Geophys. Res. 119 (4), 2550–2567, http://dx.doi.org/10.1002/2013JC009172.

Wang, Q.Y., Wang, X.W., Xie, L.L., Shang, Q.T., Lu, Y., 2014b. Observed water current and transport through Qiongzhou Strait during August 2010. Chin. J. Oceanol. Limnol. 32 (2), 703–708, http://dx.doi.org/10.1007/s00343-014-3159-6.

Waniek, J.J., 2003. The role of physical forcing in initiation of spring blooms in the northeast Atlantic. J. Mar. Syst. 39 (1–2), 57–82, http://dx.doi.org/10.1016/S0924-7963(02)00248-8.

Woodson, C.B., Eerkes-Medrano, D.I., Flores-Morales, A., Foley, M.M., Henkel, S.K., Hessing-Lewis, M., Jacinto, D., Needles, L., Nishizaki, M.T., O'Leary, J., Ostrander, C.E., Pespeni, M., Schwager, K.B., Tyburczy, J.A., Weersing, K.A., Kirincich, A.R., Barth, J.A., McManus, M.A., Washburn, L., 2007. Local diurnal upwelling driven by sea breezes in northern Monterey Bay. Cont. Shelf. Res. 27 (18), 2289–2302, http://dx.doi.org/10.1016/j.csr.2007.05.014.

Wu, M.L., Wang, Y.S., 2007. Using chemometrics to evaluate anthropogenic effects in Daya Bay, China. Estuar. Coast. Shelf Sci. 72 (4), 732—742, http://dx.doi.org/10.1016/j.ecss.2006.11.032.

Yokomizo, H., Botsford, L.W., Holland, M.D., Lawrence, C.A., Hastings, A., 2010. Optimal wind patterns for biological production in shelf ecosystems driven by coastal upwelling. Theor. Ecol. -Neth. 3 (1), 53—63, http://dx.doi.org/10.1007/s12080-009-0053-5.

Yu, W.Q., 1987. A preliminary approach of the upwelling for the northern South China Sea. Mar. Sci. 6, 7—10.